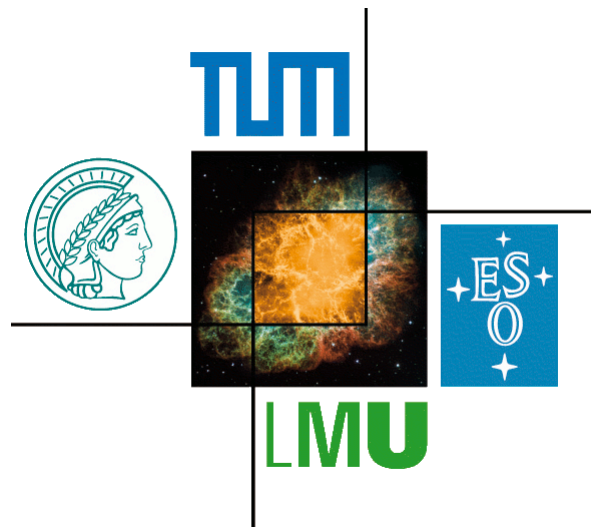


Bachelor Thesis

# Development of a cooling system for a silicon detector

PHILIP DOMINIC LOUIS

01.08.2013



Technische Universität München  
Department of Physics  
E12 / Excellence Cluster "Universe"

**First reviewer**

Prof. Dr. Laura Fabbietti

**Second reviewer**

Prof. Dr. Lothar Oberauer

**Advisors**

Joana Wirth

Rafal Lalik

# Contents

<b>Abstract</b>	<b>V</b>
<b>1 Introduction</b>	<b>1</b>
1.1 The HADES detector . . . . .	2
1.2 Physics motivation of the HADES experiment . . . . .	2
1.3 HADES and the CERBEROS upgrade . . . . .	4
<b>2 Theoretical background</b>	<b>5</b>
2.1 Principles of semiconductor detectors . . . . .	5
2.2 Temperature dependent effects of semiconductor detectors . . . . .	6
2.3 Heat transfer . . . . .	7
2.3.1 Heat radiation . . . . .	7
2.3.2 Heat conduction . . . . .	9
2.3.3 Convective heat transfer . . . . .	13
<b>3 Selection of relevant factors</b>	<b>15</b>
3.1 Technical data of the silicon detectors . . . . .	15
3.2 Heat sources . . . . .	15
3.3 Thermal conductance . . . . .	21
3.3.1 Indirect cooling . . . . .	22
3.3.2 Direct cooling . . . . .	25
3.4 Technical data of the chiller . . . . .	26
<b>4 Measurements with first prototype</b>	<b>29</b>
4.1 Temperature curves . . . . .	29
4.2 Analysis of temperature gradients . . . . .	32
4.3 Influence of readout cables . . . . .	33
4.4 Influence of leakage current . . . . .	34
<b>5 Evaluation of improvement potential</b>	<b>35</b>
5.1 Reducing temperature gradient due to heat conduction . . . . .	35
5.1.1 Direct cooling . . . . .	35
5.1.2 Indirect cooling . . . . .	38
5.2 Reducing temperature gradient due to cooling liquid flow . . . . .	42
<b>6 Experimental validation</b>	<b>45</b>
6.1 Temperature curves . . . . .	46

6.2	Analysis of temperature gradients . . . . .	48
6.3	Influence of reflecting foil . . . . .	49
<b>7</b>	<b>Summary and Outlook</b>	<b>51</b>
	<b>Bibliography</b>	<b>53</b>
	<b>Appendix</b>	<b>55</b>
	Material data . . . . .	55
	Root macro for Oosterom-Strackee algorithm . . . . .	56
	<b>Acknowledgments</b>	<b>59</b>

# Abstract

Upcoming experiments at the HADES spectrometer also include measurements with a pion beam. The secondary pion beam has a high momentum spread, which makes it mandatory to remeasure the pion momentum for the exclusive analysis. This will be done by the CERBEROS system that makes use of silicon particle detectors. To optimise the performance of these silicon detectors and to prevent them from heating up in the vacuum they will have to be cooled. In this thesis two different cooling system designs are studied. The three main characteristics are the heat sources, that have to be dissipated, the possibilities to reduce the heating of the detector and the thermal conductance between the silicon and the cooling system. Based on these characteristics the potential of both designs are compared.



# 1 Introduction

A large part of the technical innovations from the past half century are based on a deeper understanding of the principles of semiconductors. Also in the field of detector technology the achieved controllability of semiconductors is used. Certainly most devices used in the readout electronics would be unthinkable - just as the computer on which this thesis was written. But also for particle detection itself one can use semiconductor detectors (see chapter 2.1). With their help particles flying through the detector can be recognised by measuring the additional free charge carriers, generated by the particle. Due to the fact that free charge carriers are also continuously produced by thermal excitation, these detectors permanently have a background noise. By cooling the detector this noise can be reduced and additionally the radiation hardness of the detector can be increased (see chapter 2.2). In the Prof. Fabbietti group at E12, Joana Wirth dealt with these effects extensively with respect to the silicon detectors that will be used in the planned CERBEROS system at the HADES detector. One result of her bachelor thesis was that the silicon detectors have to be cooled down to  $-5^{\circ}\text{C}$  to  $-10^{\circ}\text{C}$  for optimum performance. In addition a design for a cooling system was developed and later on a concept first prototype was built.

Up to now there have been problems with the mechanical pressure the cooling system is applying to the silicon. Besides that the temperature of the silicon could only be lowered to the upper limit of the targeted temperature range. The goal of this bachelor thesis is to optimise the performance of the existing design while achieving a better control over the pressure applied on the silicon. Furthermore, an alternative design for a cooling system, which is not mechanically connected to the silicon, shall be designed and the potential of both designs shall be compared.

Finally, this bachelor thesis should answer the question, whether it is possible to reach the targeted temperature range with the investigated cooling system designs?

## 1.1 The HADES detector

The High-Acceptance DiElectron Spectrometer (HADES) is located at GSI Helmholtz-zentrum für Schwerionenforschung in Darmstadt. The HADES detector focuses on precise spectroscopy of  $e^+e^-$  pairs (dielectrons) and charged hadrons. These particles are produced by proton, pion and heavy ion induced reactions at 1 to 2 AGeV at a fixed target that is placed at half radius of the center of the RICH mirror. The particle beams are generated with the heavy-ion synchrotron SIS 18 (SchwerIonen-Synchrotron).

The HADES detector has a six folded azimuthal symmetry. The reason of this symmetry are the six superconducting coils, which produce a magnetic field with a toroidal geometry. This magnetic field deflects charged particles. The deflection is measured by the 4 Mini-Drift Chambers (MDC I/II/III/IV) with half of them located before and half of them after the magnetic field. With the deflection angle the momentum is reconstructed. For velocity measurement there are the time-of-flight scintillator walls (TOF/TOFINO). With the Ring Imaging Cherenkov detector (RICH) in conjunction with the electromagnetic shower detectors (Pre-Shower) the electron identification is performed. This is possible since in the SIS 18 energy regime only electrons are fast enough to produce Cherenkov photons. Additionally there is a diamond START detector placed in front of the target to determine the reaction time. The setup can be seen in figure 1.1.

The whole setup allows to detect particles with an polar angle between  $\theta = 18^\circ$  and  $\theta = 85^\circ$ . In this range it has an azimuthal acceptance of 85%. [1]

## 1.2 Physics motivation of the HADES experiment

HADES is designed to study modifications of properties of hadrons inside a strongly interacting medium. It has been specifically optimised to measure modifications of the light vector mesons  $\rho$ ,  $\omega$ ,  $\phi$ , because they have a lifetime comparable to the compression time of heavy-ion reactions generated by the SIS 18. Additionally they decay into  $e^+e^-$  pairs, which are not influenced by the strong interaction and therefore provide undistorted information of the vector mesons inside the baryonic matter.

These observables should be studied also employing pion-beams, to investigate the properties of the hadron at normal nuclear matter density. Of particular interest are also the properties of strange baryons and mesons, which could teach us something quantitative about the meson-baryon interaction as a function of different system densities.

This includes the interaction of strange mesons like  $K_s^0$  with nuclear matter as well as precision measurements of strange baryons like  $\Sigma(1385)$  and  $\Lambda(1405)$ . Especially for the measurements with strange mesons it is an advantage that the pions transfer

only a low momentum. So the produced mesons and baryons decay when they are still inside the nucleus, thus providing better information about modifications due to the surrounding strong interacting medium. [1, 2]

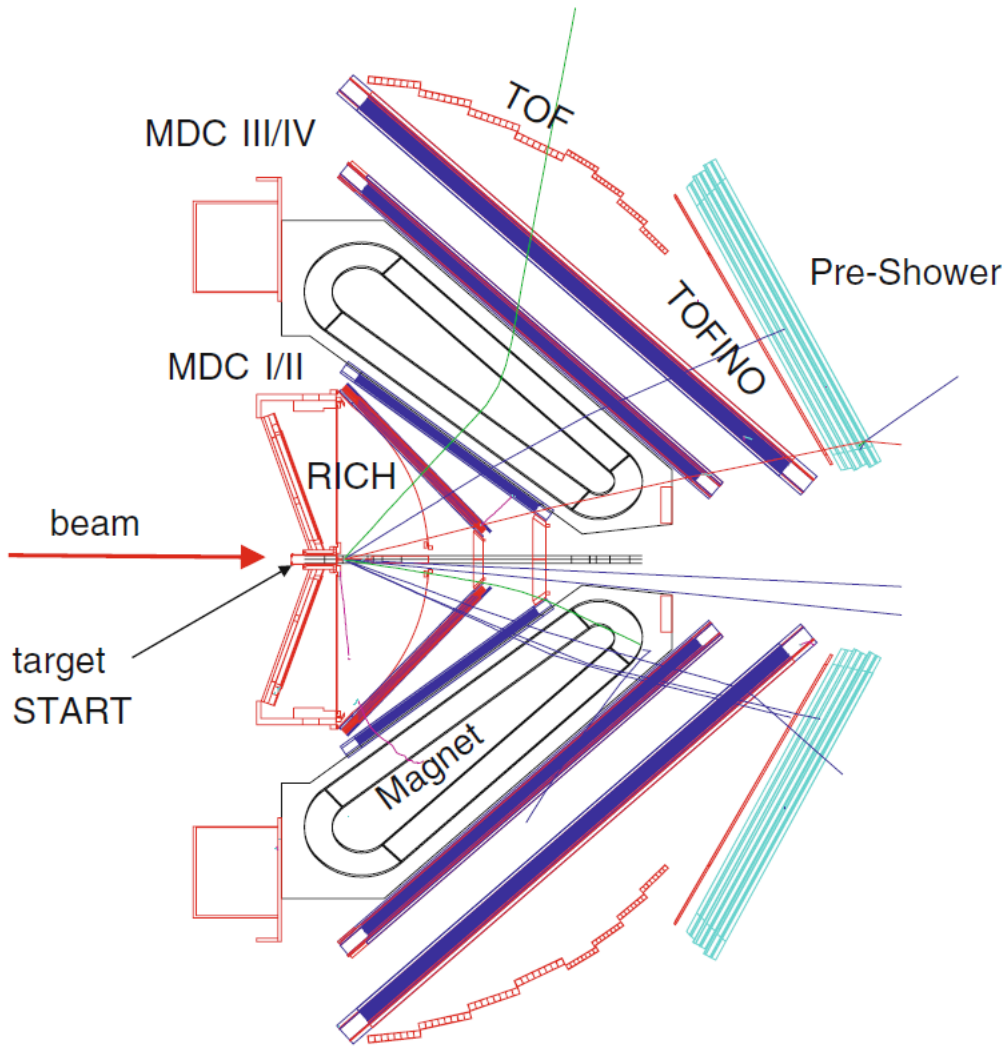


Figure 1.1: Sketch of the HADES detector with all its components. First after the target is the Ring Imaging Cherenkov detector (RICH). Then there are 4 Mini-Drift Chambers (MDC I/II/III/IV) located before and after the superconducting magnet. Followed by time-of-flight scintillator walls (TOF/TOFINO) and finally the electromagnetic shower detectors (Pre-Shower).

### 1.3 HADES and the CERBEROS upgrade

A pion production target has been installed at the heavy-ion synchrotron. This makes it possible to study elementary pion-induced reactions, which is a prerequisite for understanding the complex heavy-ion collisions. A problem is that the pion beam has a high momentum spread ( $\frac{\Delta p}{p} = \pm 6\%$ ) due to its secondary nature. The the only detector the pions are traveling through is the diamond START detector and it can only be used for measuring time-stamps. This makes it mandatory to remeasure the pion momentum with a new alternative detector concept. The Central BEam tRacker for piOnS (CERBEROS) measures the position of the particles at two point in the dispersive plane of the beam line leading from the production target to the HADES target (see figure 1.2). The position of the particles in the dispersive plane depends on the deflection angle in the dipole magnets, which is dependent on the momentum of the pions. Therefore the pion momentum can be reconstructed using the information of the pion's position. For measuring the position of the particles two silicon detectors are used. [1]

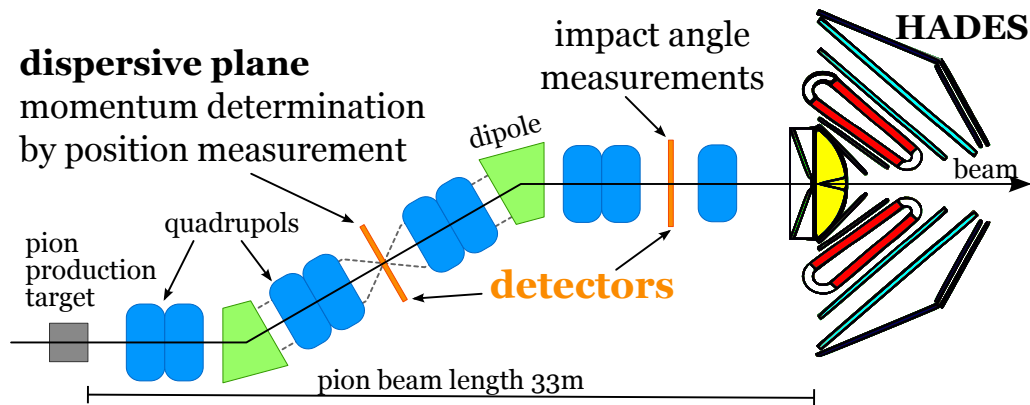


Figure 1.2: Sketch of the beam line from the pion production target to the HADES detector. The positions of the CERBEROS detectors are shown.

## 2 Theoretical background

### 2.1 Principles of semiconductor detectors

A semiconductor detector makes use of the properties of a p-n junction. A p-n junction describes the transition from a p-doped semiconductor to a n-doped semiconductor. At the point of contact the fermi levels equalise as electron from the n-type and holes from the p-type material annihilate and form a space charge region with no free charge carriers left inside. Therefore the charged donors and acceptors are uncompensated and generate an intrinsic electric field between them. This bends the band structure in a way that the diffusion current and drift current of both electrons in the conduction band and holes in the valence band are in an equilibrium state. Electron hole pairs thermally generated in the space charge region are separated by the intrinsic electromagnetic field and can not recombine. This generates the drift current, which is also named generation current.

When an external voltage is applied in reverse bias the space charge region is enlarged. With increasing voltage the diffusion current is exponentially suppressed, leaving the generation current uncompensated. At the depletion voltage of a semiconductor detector the space charge region is filling the whole volume and the uncompensated generation current is called leakage current of the detector. The current from thermally generated electron hole pairs is called leakage current, because the way of measuring particles flying through the detector is to measure the electron hole pairs generated with the energy transferred to the silicon by the particles flying through the detector. So the measured signal is the current flowing in reverse bias. The true signal of the particles is always disturbed by the generation current or leakage current.

To get a spatial resolution both detector surfaces are covered with charge collection electrodes in form of strips. The generated electron hole pairs are normally collected by one or two strips [3]. So by reading out all strips of one side allows to define the location of a particle in one dimension. If the strips on the two sides are perpendicular to each other the combined information of the readout allows to reconstruct the location where the particle crossed the detector.

## 2.2 Temperature dependent effects of semiconductor detectors

There are several effects in semiconductor detectors that show strong temperature dependence. The following effects explain the importance of a cooling system.

**Leakage current** The leakage current is the current that is generated by thermally excitation of electron-hole pairs. The high tail of the Boltzmann distribution is responsible for this excitation. Therefore it is strongly temperature dependent. The exact dependency is described by following formula [4]:

$$I_{LC} \propto T^2 \exp\left(-\frac{E_g}{2 \cdot k_B \cdot T}\right) \quad (2.1)$$

with band gap energy  $E_g$ , Boltzmann constant  $k_B$  and temperature  $T$ . This dependency is visualized for silicon ( $E_g = 1.12$  eV) in figure 2.1.

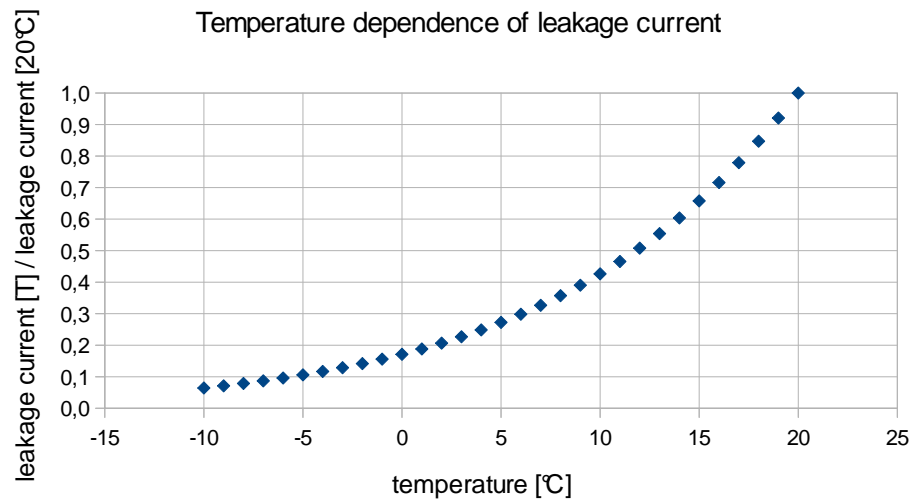


Figure 2.1: The graph shows the temperature dependence of the leakage current of silicon. Leakage current is given in comparison to the leakage current at room temperature ( $20^\circ\text{C}$ )

**Radiation hardness** With lower temperature the damage caused by radiation is reduced. The radiation creates primary 0D- Frenkel defects, interstitials and vacancies, in the lattice structure. Primary defects are mobile and can drift through the silicon. Over time primary defects can form electrically active clusters that are more harmful than the isolated primary defects, which it results from, combined. This clustering effect is called reverse annealing and it slowly but more or less temporary increases the leakage current. Since the

mobility of the primary defects depends on thermal energy cooling slows down the growth of harmful clusters. Considering that the detectors must operate over a longer timescale and are exposed to the high intensity beam this effect is of importance.

In conclusion it can be said that cooling a semiconductor detector is important, since lower temperatures are very advantageous for the operation of a semiconductor detector. First of all the leakage current is strongly reduced, what helps keeping noise small and therefore improves signal to background ratio. Secondly harmful clustering and the associated permanent rise in leakage current is slowed down. This allows operating the detector on a longer timescale.

## 2.3 Heat transfer

### 2.3.1 Heat radiation

Every body with a temperature above absolute zero emits electromagnetic radiation. This can be explained by the fact, that thermal energy is kinetic energy of randomly moving/oscillating particles. Moving particles that scatter result in charge-acceleration and oscillating particles result in dipole-oscillations. In both cases electromagnetic waves are emitted which can be absorbed by other bodies. Consequently opposing pieces of matter without any connection can still exchange energy.

#### Black body

Black bodies are bodies that completely absorb electromagnetic radiation. Its principles are described by PLANCK'S LAW, which is obtained from statistical mechanics with the assumption of a quantized electromagnetic field.  $I(\nu, T)$  and  $I(\lambda, T)$  are the amount of energy per unit surface area per unit time per unit solid angle emitted at frequency  $\nu$  or wavelength  $\lambda$  in direction of the surface normal.

$$I(\nu, T) = \frac{2 \cdot h \cdot \nu^3}{c^2} \cdot \frac{1}{\exp\left(\frac{h\nu}{k_B T}\right) - 1} \quad (2.2)$$

$$I(\lambda, T) = \frac{2 \cdot h \cdot c^2}{\lambda^5} \cdot \frac{1}{\exp\left(\frac{hc}{\lambda k_B T}\right) - 1} \quad (2.3)$$

with Planck constant  $h$  and light speed  $c$ .

The energy emitted under an angle  $\Theta$  to the surface normal is proportional to the effective area seen under this angle. This is explained by LAMBERT'S COSINE LAW, which assumes that the brightness, the luminous energy per solid angle, for observers at the same distances is independent of the angle  $\Theta$  of the observers to the surface normal. Since the solid angle covered by an area<sup>1</sup> is proportional to  $\cos \Theta$ , the energy emitted from the area under the angle  $\Theta$  has to be proportional to  $\cos \Theta$  too.

$$I(\nu, T, \Theta) = I(\nu, T) \cdot \cos \Theta \quad (2.4)$$

The STEFAN-BOLTZMANN LAW can be obtained by integrating 2.4 over all frequencies.

$$P(T) = \int_{half\ space} \int_0^\infty I(\nu, T, \Theta) d\nu d\Omega \cdot \int_{surface} dA$$

$$P(T) = \int_0^\infty \frac{2 \cdot h \cdot \nu^3}{c^2} \cdot \frac{1}{\exp\left(\frac{h\nu}{k_B T}\right) - 1} d\nu \cdot \int_0^{2\pi} d\varphi \int_0^{\frac{\pi}{2}} \cos \Theta \sin \Theta d\Theta \cdot \int_{surface} dA$$

By substituting  $a = \frac{h\nu}{k_B T}$  one obtains following expression:

$$P(T) = \frac{2 \cdot k_B^4 \cdot T^4}{c^2 \cdot h^3} \cdot \underbrace{\int_0^\infty \frac{a^3}{\exp(a) - 1} da}_{\frac{\pi^4}{15}} \cdot \underbrace{\int_0^{2\pi} d\varphi \int_0^{\frac{\pi}{2}} \cos \Theta \sin \Theta d\Theta}_{\pi} \cdot \underbrace{\int_{surface} dA}_A$$

$$P(T) = \frac{2 \cdot \pi^5 \cdot k_B^4}{15 \cdot c^2 \cdot h^3} \cdot A \cdot T^4 = \sigma \cdot A \cdot T^4 \quad (2.5)$$

with Stefan–Boltzmann constant  $\sigma$ .

With equation 2.5 the total power emitted from a surface with area  $A$  and temperature  $T$  can be calculated and in addition the absorbed power to a surface with area  $A$  from an ambient radiation at temperature<sup>2</sup>  $T$ . This can be explained by a thought experiment. The solid angle over the area  $A$  is filled with material at temperature  $T_1$ . In thermal equilibrium the area also has temperature  $T_1$  and emitted and absorbed power on the surface is equal. In conclusion we can calculate the absorbed power for this case. If the area has another temperature  $T_2$  the absorbed power stays the same since heat radiation photons do not interact<sup>3</sup>.

<sup>1</sup>The area has to be small compared to the distance of the observer to the area.

<sup>2</sup>Radiation at temperature  $T$  is emitted from bodies with the temperature  $T$ .

<sup>3</sup>At least not in an amount that would be of any importance.

### Gray body

For non-black bodies, which do not completely absorb electromagnetic radiation, the emissivity  $\varepsilon$  ( $0 \leq \varepsilon \leq 1$ ) has to be considered. The emissivity corresponds to the amount of energy absorbed from the total incoming electromagnetic radiation power. In general the emissivity is frequency dependent, but since only a small spectrum is important for heat radiation at room temperature we assume  $\varepsilon$  as constant. This approximation is called gray body approximation. The thought experiment used for black bodies also works for gray bodies. It gives us that in thermal equilibrium the absorbed and emitted power is the same. Therefore also the emitted energy scales with  $\varepsilon$ . This is why  $\varepsilon$  is called emissivity.

$$P(T) = \varepsilon \cdot \sigma \cdot A \cdot T^4 \quad (2.6)$$

Equation 2.6 is the Stefan-Boltzmann Law for gray bodies and it can be used to calculate the emitted as well as the absorbed power on an area  $A$  of a gray body.

### 2.3.2 Heat conduction

In general heat conduction is described by the following partial differential equation [5]:

$$\rho(\vec{r}) \cdot c(\vec{r}) \cdot \frac{\partial T(\vec{r}, t)}{\partial t} = \nabla[\lambda(\vec{r}) \cdot \nabla T(\vec{r}, t)] + P(\vec{r}) \quad (2.7)$$

with mass density  $\rho$ , specific heat capacity  $c$ , temperature  $T$ , thermal conductivity  $\lambda$  and heat sources  $P$ .

There is often no analytical solution for this equation. For technical relevant heat conductance calculations this equation is nowadays solved by computers using finite element methods. This will be explained and used in section 3.3.1.

For a stationary case in homogenous material without heat sources the equation 2.7 can be used to define a heat flux density  $\vec{q}$  [5]:

$$\vec{q} = -\lambda \cdot \nabla T \quad (2.8)$$

By integrating equation 2.8 over a cross sectional area of a body one obtains the heat flux  $\Phi$  through this surface.

$$\Phi = -\lambda \cdot \oint_{\text{surface}} \nabla T \cdot d\vec{A} \quad (2.9)$$

## Heat conduction in a 1 dimensional geometry

Assuming a material of 1 dimensional geometry and cross sectional area  $A$  between two contact surfaces at constant temperature the integral in 2.9 can be solved:

$$\Phi = -\lambda \cdot A \cdot \frac{\Delta T}{x} \quad (2.10)$$

with heat flux  $\Phi$ , cross sectional area  $A$  and distance between contact surfaces  $x$ .

With this equation we can define a thermal conductance  $\sigma_Q$  and a thermal resistance  $R_Q$ , analogue to electric conductance and resistance in electrodynamics:

$$\sigma_Q = \frac{\Phi}{-\Delta T} \longrightarrow \sigma_Q = \lambda \cdot \frac{A}{x} \quad (2.11)$$

$$R_Q = \frac{-\Delta T}{\Phi} \longrightarrow R_Q = \frac{1}{\lambda} \cdot \frac{x}{A} \quad (2.12)$$

In series connection and parallel connection of heat conductors, the total thermal conductance and thermal resistance can be calculated with the same rules that apply in electrodynamics.

series connection	parallel connection
$R_{Q,total} = \sum_i R_{Q,i}$	$\frac{1}{R_{Q,total}} = \sum_i \frac{1}{R_{Q,i}}$
$\frac{1}{\sigma_{Q,total}} = \sum_i \frac{1}{\sigma_{Q,i}}$	$\sigma_{Q,total} = \sum_i \sigma_{Q,i}$

Table 2.1: Formulas to solve series connections and parallel connections of thermal resistors.

Using equation 2.11 and 2.12 the heat flux through materials with a 1 dimensional geometry can be easily calculated. It is often possible to approximate other structures whose cross sectional area perpendicular to the temperature gradient is constant and whose minimum and maximum distance between contact surfaces along the temperature gradient is approximately the same.

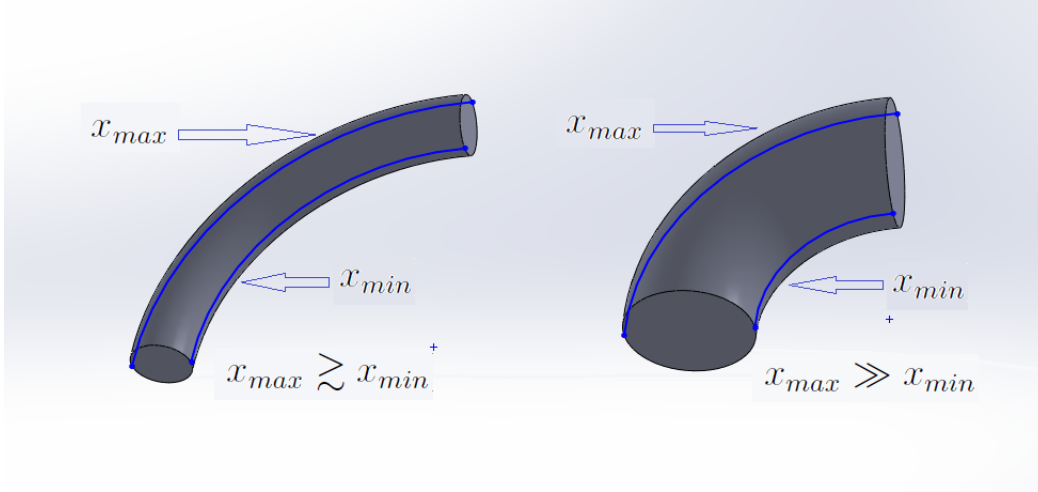


Figure 2.2: Illustration of cases in which approximation with equation 2.10 is possible (left,  $x_{max} \gtrsim x_{min}$ ), not possible (right,  $x_{max} \gg x_{min}$ ).

### Heat conduction in a cylindrical geometry

A shape that cannot be approximated that way is a body with a cylindrical geometry and an inner and outer temperature, e.g. a pipe. This will be needed to calculate the heat flux through the isolation of the cooling liquid pipes outside the vacuum chamber. Taken a pipe with inner radius  $r_{in}$ , outer radius  $r_{out}$  and length  $l$ . If  $r_{out} \gtrsim r_{in}$  the surface through which the heat is conducted  $A = 2\pi \cdot r \cdot l$  does not stay the same. The pipe can be seen as  $N$  thinner pipes stuck into each other. This corresponds to a series of many heat conductors.

$$r_{in,i} = r_{out,i-1} \text{ for } i \in [2, 3, \dots, N] \text{ and } r_{in} = r_{in,1}, r_{out} = r_{out,N}$$

If  $N \gg 1$  the following approximations can be made:

$$\bar{r}_i \approx r_{out,i} \approx r_{in,i}, \Delta r_i = r_{out,i} - r_{in,i}$$

$$R_Q = \sum_{i=1}^N R_{Q,i} = \sum_{i=1}^N \frac{1}{\lambda} \cdot \frac{x_i}{A_i} \approx \sum_{i=1}^N \frac{1}{\lambda} \cdot \frac{\Delta r_i}{2\pi \cdot \bar{r}_i \cdot l}$$

$$\xrightarrow{N \rightarrow \infty} R_Q = \int_{r_{in}}^{r_{out}} \frac{1}{\lambda} \cdot \frac{dr}{2\pi \cdot r \cdot l} = \frac{1}{2\pi \cdot \lambda \cdot l} \ln\left(\frac{r_{out}}{r_{in}}\right) \quad (2.13)$$

$$\sigma_Q = \frac{1}{R_Q} = 2\pi \cdot \lambda \cdot l \cdot \frac{1}{\ln\left(\frac{r_{out}}{r_{in}}\right)} \quad (2.14)$$

### Temperature dependence of heat conductivity $\lambda$

The thermal conductivity  $\lambda$  is a material specific property which in general depends on the temperature. The effect of temperature is different for metals and nonmetals. Both will be discussed here shortly.

- *Metals: Electron heat conduction*

In metals the heat is primarily conducted by free electrons. The WIEDEMANN–FRANZ LAW tells us that the thermal conductivity at higher temperature is roughly proportional to the absolute temperature and the electrical conductivity. Since for room temperature in pure metals the electrical conductivity decreases with temperature the thermal conductivity stays approximately constant.

$$\frac{\lambda}{\sigma_{el}} = \frac{\pi^2}{3} \cdot \left(\frac{k_B}{q_e}\right)^2 \cdot T \longrightarrow \lambda \propto \sigma_{el} \cdot T \quad (2.15)$$

with electrical conductance  $\sigma_{el}$  and electron charge  $q_e$

The result of the theoretically expected behavior for pure metals for the whole temperature range is[6]:

$$\lambda \propto \begin{cases} T & \text{for } T \lll \Theta_D \\ T^{-4} & \text{for } T \ll \Theta_D \\ \text{const} & \text{for } T \gg \Theta_D \end{cases} \quad (2.16)$$

The Debye-Temperature  $\Theta_D$  of most metals is near room temperature (*Cu* :  $\Theta_D = 343$  K, *Al* :  $\Theta_D = 428$  K). For impure metals and alloys the rise for  $T \ll \Theta_D$  is completely suppressed. So for pure metals the thermal conductivity is slowly increasing with lower temperatures, for impure metals and alloys the thermal conductivity is slightly decreasing with lower temperatures.

- *Nonmetals: Phonon heat conduction*

In nonmetals the heat is conducted by phonon which are quasi particle to describe lattice vibrations. The number of phonon is proportional to  $T^3$ . The mobility of phonon decreases due to scattering processes.

Point defect scattering: Dependent on the point defect concentration. Thus this effect is often temperature independent.

Phonon-phonon scattering: There are two types of three-phonon-processes, the Normal-scattering and the Umklapp-scattering. Since Normal-scattering maintains the phonon momentum they do not obstruct heat conduction. Therefore only Umklapp-scattering is important.

The result of the theoretically expected behavior is[6]:

$$\lambda \propto \begin{cases} T^3 & \text{for } T \lll \Theta_D \text{ (ph-defect-scattering)} \\ T^n \cdot e^{\frac{\Theta_D}{T}}, n \simeq 0 - 3 & \text{for } T \ll \Theta_D \text{ (ph-ph-scattering)} \\ \frac{1}{T} & \text{for } T \gg \Theta_D \text{ (ph-ph-scattering)} \end{cases} \quad (2.17)$$

Since the Debye-Temperature  $\Theta_D$  of most nonmetals is near room temperature or somewhat higher (*Si* :  $\Theta_D = 645$  K, *Ge* :  $\Theta_D = 374$  K), the thermal conductivity at room temperature is decreasing proportional to  $1/T$  or faster.

For the task of the cooling system the assumption of a constant thermal conductivity is sufficient. The material with the biggest change in thermal conductivity should be silicon. The change is approximately 10% between  $-10^\circ\text{C}$  and  $20^\circ\text{C}$ .

### 2.3.3 Convective heat transfer

In contrast to the other ways of heat transfer, convective heat flow is always linked to a mass flow. This implies that convective heat transfer only occurs in combination with liquids or gases. The difference to heat conduction can be further explained with following example.

A warm body surrounded by a fluid creates a layer of warm fluid in the contact area. This heat transfer takes place via heat conduction. In a perfectly calm fluid the layer can get thicker, spreading the temperature gradient over a longer distance  $x$ , which reduces the heat flux  $\Phi$ (see 2.10). The fluid forms an isolating layer around the body. In the case that the fluid moves the warm layer around the body is constantly swept away and replaced with cold fluid. The heat of the boundary layer is mixed into the whole fluid flow and gets carried away. This increases the heat flow from the body to the fluid since the temperature now changes over a much shorter distance. Additionally the flow behavior in the boundary layer is very different for laminar and turbulent fluid flow, which can be described by fluid mechanics.

Furthermore the flow of the fluid can either be caused by forced convection or natural convection. In forced convection an externally generated pressure gradient is causing the stream. In this case the flow is normally not dependent on the temperature. Natural convection denotes the phenomenon, that warm fluids normally have a lower density. This creates a buoyant force that leads to a stream of warm fluid going upwards and a cold stream going in opposite direction.



## 3 Selection of relevant factors

### 3.1 Technical data of the silicon detectors

There are two silicon detectors that were important in the development of the cooling system. The pion tracker detector is the one that will be used in the CERBEROS system. This is the detector the cooling system is build for. Additionally for test purposes a silicon detector from the SiAVio experiment was used. The advantage of the SiAVio detector is, that they are less expensive and some spares are existing.

Both silicon detectors are double sided 90° strip detectors. This means that there are strips on both sides that are perpendicular to each other.

	SiAVio	pion tracker
active area	4.4 cm × 6.4 cm	10.4 cm × 10.4 cm
strips	40 × 60	128 × 128
strip covered area	4.0 cm × 6.0 cm	9.7 cm × 9.7 cm
thickness	1000 μm	300 μm
depletion voltage	250 V	110 V
PCB material		FR 4
Bulk doping	n-type	p-type

Table 3.1: Technical data of the silicon detector

### 3.2 Heat sources

For the development of a cooling system it is mandatory to know the amount of heat that has to be dissipated. Therefore all the different heat sources as well as their importance will be discussed in this section. All the calculations will be done for the SiAVio prototype (short: *Sil*) as well as the pion tracker detector of CERBEROS (short: *PT*).

The heat-flow is often dependent on the temperature gradient. In these cases the temperatures that are planned to be achieved will be used ( $T_{cooling} = -15^{\circ}\text{C}$ ,  $T_{silicon} = -10^{\circ}\text{C}$ ).

## Leakage current

As already discussed the leakage current of a silicon detector is an important characteristic. But besides that it is also a heat source that depletes energy in the detector. The amount of energy equals the current times the voltage drop over the detector. In operation the voltage drop over the detector equals the depletion voltage.

$$P_{Sil}^{LC} = 2.5 \mu\text{A} \cdot 250 \text{ V} = 625 \mu\text{W}$$

$$P_{PT}^{LC} = 2 \mu\text{A} \cdot 110 \text{ V} = 220 \mu\text{W}$$

## Particle flux

Each particle going through the detector loses some energy. This degradation of energy is used for the detection of the particles. But most of this energy is transferred into heat. Here not only the energy used to create electron-hole pairs is important but the whole energy loss in the silicon. The total energy loss equals the flux multiplied by the energy deposited per particle which can be calculated using the restricted Bethe-Bloch formula for thin layers [7].

$$P_{PT}^{PF} = 10^8 \frac{\text{particles}}{\text{s}} \cdot 80 \frac{\text{keV}}{\text{particle}} = 1.3 \mu\text{W}$$

## Heat conduction through readout cables

### SiAVio

The SiAVio readout cables are normal shielded data cables. The cables are connected to the readout PCB of the SiAVio detector. Therefore the heat is not directly transferred to the silicon. Since it is not possible to estimate the conductance of the readout PCB and the detector PCB with their imprinted circuits, just the heating through the cables to the connectors on the readout PCB is calculated.

There are 3 readout cables with a length of 85–90 cm. Each containing 25 copper wires with a diameter of 0.3–0.4 mm and 190–210 iron threads with a diameter of 0.15–0.2 mm that are wadded around the data cables for shielding.

SiAVio	copper cables (1 cable)	iron threads (1 cable)	total (3 cables)
distance $x$	850–900 mm	850–900 mm	-
cross sectional area $A$	1.77–3.14 mm <sup>2</sup>	3.36–6.60 mm <sup>2</sup>	-
thermal conductivity $\lambda$	400 $\frac{\text{W}}{\text{m}\cdot\text{K}}$	80 $\frac{\text{W}}{\text{m}\cdot\text{K}}$	-
thermal conductance $\sigma_Q$	0.79–1.48 $\frac{\text{mW}}{\text{K}}$	0.30–0.62 $\frac{\text{mW}}{\text{K}}$	3.27–6.30 $\frac{\text{mW}}{\text{K}}$

The heat flux from a 20°C vacuum chamber to a –15°C cooling structure is:

$$P_{Sil}^{RC} = 115 - 220 \text{ mW}$$

### Pion tracker

The readout cables are made of thin copper stripes sheathed by kapton. The heating through the readout cables is almost directly transferred to the silicon via the bondings, because the connectors are less than 1 cm away from the silicon. To calculate the heat conduction we have to know the profile and the length of the cables. The copper stripes on the kapton are 35–40  $\mu\text{m}$  thick and there are 32 thin stripes (width: 0.15 mm) 2 medium stripes (width: 0.4 mm) and 2 broad stripes (width: 1.2 mm). The kapton has a thickness of 70–90  $\mu\text{m}$  and a width of 20–23 mm. In total there are 8 of these readout cables.

pion tracker	kapton tape (1 cable)	copper stripes (1 cable)	total (8 cables)
distance $x$	100–150 mm	100–150 mm	-
cross sectional area $A$	1.40–2.07 mm <sup>2</sup>	0.28–0.32 mm <sup>2</sup>	-
thermal conductivity $\lambda$	0.12–0.37 $\frac{\text{W}}{\text{m}\cdot\text{K}}$	400 $\frac{\text{W}}{\text{m}\cdot\text{K}}$	-
thermal conductance $\sigma_Q$	0.001–0.008 $\frac{\text{mW}}{\text{K}}$	0.747–1.280 $\frac{\text{mW}}{\text{K}}$	5.98–10.30 $\frac{\text{mW}}{\text{K}}$

The heat flux from a 20°C vacuum chamber to a –10°C detector is:

$$P_{PT}^{RC} = 180\text{--}310 \text{ mW}$$

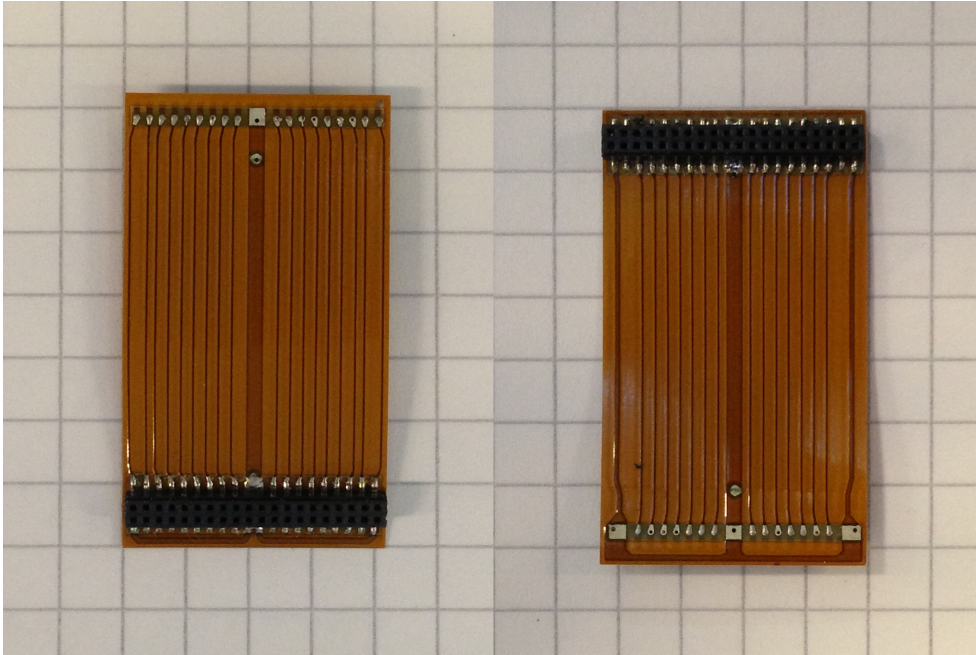


Figure 3.1: sample readout cable (front and back) of the pion tracker detector, the copper stripes are identical to the final design but the length is shorter

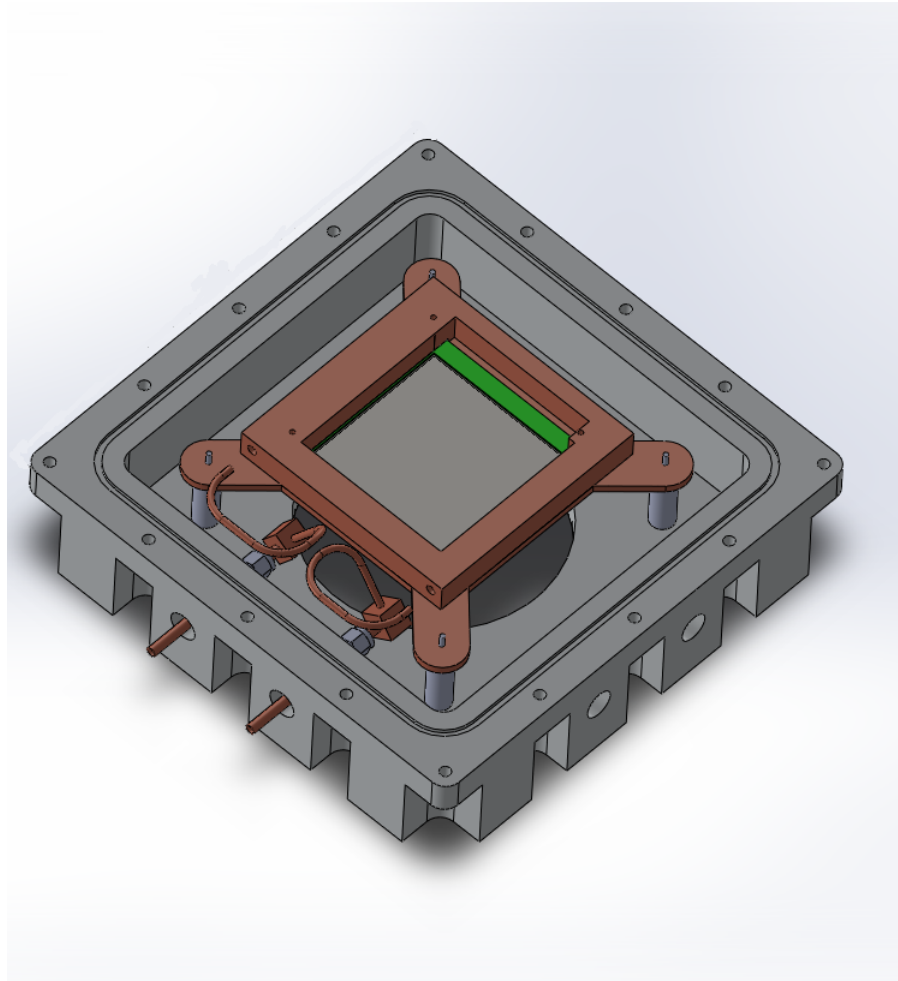


Figure 3.2: One half of the vacuum chamber and the indirect cooling for the pion tracker detector mounted on 4 pillars.

### Heat conduction through support pillars

The support structure that is needed to mount the cooling structure inside the vacuum chamber will also conduct heat. Since the existing support structures of the SiAVio and pion tracker prototype cooling systems are temporary solutions only heat conduction through the support structure of the final pion tracker setup will be estimated.

The support structure of the final setup will consist of 4 pillars with a length of 43 mm. The maximum heat conduction from the 20°C vacuum chamber to the -15°C cooling structure depends on the material used and the thickness of the pillars. Moreover the material has to be stable enough to hold up to 2–4 kg. Possible candidates of suitable materials are:

**Heavily alloyed steel** It combines high stability with a medium heat conductiv-

ity ( $\lambda = 15\text{--}35 \frac{\text{W}}{\text{m}\cdot\text{K}}$ ). The heat conductivity is significantly lower than those from pure metals, since the impurity makes it harder for the phonon to travel through the material. Due to the high stability the pillars could have a diameter of 5–8 mm. For pillars of this material a heat flow of 1000–6000 mW has to be expected.

**Delrin** Delrin is a polyoxymethylene (POM) also known as engineering thermoplastic. For a synthetic polymer it has a high stiffness and good dimensional stability. This makes it possible to use it as a material for pillars with a diameter of 12–15 mm. The low heat conductivity ( $\lambda = 0.30\text{--}0.37 \frac{\text{W}}{\text{m}\cdot\text{K}}$ ) reduces the heat flow to  $P_{PT}^{SP} = 110\text{--}210$  mW. Therefore delrin is the preferred material.

## Ambient radiation

The whole setup exchanges heat via radiation. Since all occurring temperatures are between 250–300 K the majority of this heat radiation is in the infrared spectrum. The emissivity  $\varepsilon$  for materials used is in the appendix. Since the emissivity of metals changes with oxidation the used values are often estimations.

### Si $\wedge$ Vio

The surfaces of both sides of the Si $\wedge$ Vio detector is  $A_{Sil} = 2 \cdot 4.4 \text{ cm} \cdot 6.4 \text{ cm} = 56.3 \text{ cm}^2$ . Using the Stefan-Boltzmann law 2.6 the heat radiation power to this surface from a  $T_1 = 20^\circ\text{C}$  ambient radiation to a  $T_2 = -10^\circ\text{C}$  detector is:

$$P_{Sil,total}^{AR} = \varepsilon \cdot \sigma \cdot A_{Sil} \cdot (T_1^4 - T_2^4) = \varepsilon \cdot (2.36 \text{ W} - 1.53 \text{ W}) = \varepsilon \cdot 0.83 \text{ W}$$

The surface of the silicon is covered with aluminium strips with a width of  $950 \mu\text{m}$  and a distance of  $50 \mu\text{m}$  between them. The emissivity of the detector surface is interpolated from the emissivities of aluminium ( $\varepsilon = 0.04\text{--}0.09$ ) and silicon ( $\varepsilon = 0.83\text{--}0.96$ ) weighted with the surface shares. This gives an emissivity of the detector of  $\varepsilon = 0.08\text{--}0.13$ .

$$P_{Sil}^{AR} = 70\text{--}110 \text{ mW}$$

Since the mounting structure of the Si $\wedge$ Vio prototype is made of plastic the emissivity is much higher than those of metals ( $\varepsilon = 0.90\text{--}0.95$ ). But on the other side the thermal conductivity is much lower ( $\lambda \approx 0.3 \frac{\text{W}}{\text{m}\cdot\text{K}}$ ). So energy, which is absorbed more than some centimeters away from the silicon, is not conducted to the cooling liquid well. Instead it heats up the plastic, which leads to a higher emitted heat radiation power. This makes it difficult to calculate the heating by absorbed heat radiation. An idea how to estimate the heating is to define an effective surface area in which the absorbed heat is conducted to the cooling liquid. So just the surface not more than 1–3 cm away from the silicon, is counted to the effective area. The effective surface area of the pion tracker mounting structure is

$A_{mount,eff} \approx 2 \cdot (2 \cdot 4.4 \text{ cm} + 2 \cdot 6.4 \text{ cm}) \cdot (1-3) \text{ cm} = 45-130 \text{ cm}^2$ . For a  $T_1 = 20^\circ\text{C}$  ambient radiation and a  $T_2 = -15^\circ\text{C}$  mounting structure the heating power is:

$$P_{Sil,mount,total}^{AR} \approx \varepsilon \cdot \sigma \cdot A_{mount,eff} \cdot (T_1^4 - T_2^4) = \varepsilon \cdot (0.75-2.25) \text{ W}$$

$$P_{Sil,mount}^{AR} \approx 700-2100 \text{ mW}$$

### Pion tracker

The detector surfaces of the both sides of the pion tracker detector is  $A_{PT} = 2 \cdot 10 \text{ cm} \cdot 10 \text{ cm} = 200 \text{ cm}^2$ . Using the Stefan-Boltzmann law 2.6 the heat radiation power to this surface from a  $T_1 = 20^\circ\text{C}$  ambient radiation to a  $T_2 = -10^\circ\text{C}$  detector is:

$$P_{PT,total}^{AR} = \varepsilon \cdot \sigma \cdot A_{PT} \cdot (T_1^4 - T_2^4) = \varepsilon \cdot (8.38 \text{ W} - 5.44 \text{ W}) = \varepsilon \cdot 2.94 \text{ W}$$

The surface of the silicon is covered with aluminium strips with a width of  $700 \mu\text{m}$  and a distance of  $60 \mu\text{m}$  between them. The emissivity of the detector surface is interpolated from the emissivities of aluminium ( $\varepsilon = 0.04-0.09$ ) and silicon ( $\varepsilon = 0.83-0.96$ ) weighted with the surface shares. This gives an emissivity of the detector of  $\varepsilon = 0.10-0.16$ .

$$P_{PT}^{AR} = 300-470 \text{ mW}$$

The surface area of the pion tracker cooling structure is  $A_{Mount} = 400-500 \text{ cm}^2$  (see 3.4). For a  $T_1 = 20^\circ\text{C}$  ambient radiation and a  $T_2 = -15^\circ\text{C}$  cooling structure the heating power is:

$$P_{PT,cooling,total}^{AR} = \varepsilon \cdot \sigma \cdot A_{Mount} \cdot (T_1^4 - T_2^4) = \varepsilon \cdot 6.68-8.35 \text{ W}$$

The cooling structure is made of copper and was slightly polished ( $\varepsilon = 0.12-0.15$ ) when manufactured. But over time the surface oxidised and became dull. So the emissivity has increased. A rough estimation is  $\varepsilon \approx 0.3-0.5$ .

$$P_{PT,cooling}^{AR} = 2000-4100 \text{ mW}$$

### Summary

Heat sources which heat up the detector and the holding structure have been discussed. A summary can be seen in the tables.

The mayor heat sources are heat radiation and thermal conduction through readout cables. These two heat sources will be in the focus in section 5.1.2, where the possibilities to reduce the heating power will be analysed.

In how far the heating power to the mounting structure is transferred to the cooling liquid or the silicon will additionally influence the temperature of the detector. This effect will be important in section 4.2.

Heat source	heating power to detector	heating power to cooling
leakage current	220 $\mu\text{W}$	
particle flux	1.3 $\mu\text{W}$	
readout cables	180–310 mW	
support pillars		110–210 mW
ambient radiation	200–470 mW	2000–4000 mW
total	380–780 mW	2100–4200 mW

Table 3.2: Heat sources in pion tracker setup

Heat source	heating power to detector	heating power to mounting
leakage current	625 $\mu\text{W}$	
particle flux		
readout cables		115–220 mW
ambient radiation	70–110 mW	700–2100 mW
total	70–110 mW	800–2300 mW

Table 3.3: Heat sources in SiAVio setup

### 3.3 Thermal conductance

The cooling liquid is piped inside the vacuum chamber to cool the cooling structure. From that point the cooling takes place by heat conduction through solid materials.

There are two different approaches for the cooling structure, which conducts the heat from the detector to the cooling fluid:

*Indirect cooling:* In the indirect cooling the PCB, to which the detector is attached, is the only part that touches the silicon. The heat has to be transferred through the PCB to the copper mounting blocks, which are pressed on both sides of the PCB. The advantage is that the sensitive silicon detector is not touched. One disadvantage is that the PCB is even colder than the silicon. Since the thermal expansion coefficient of silicon ( $\alpha_T = 2.6 \cdot 10^{-6} \text{ 1/K}$ ) is much lower than the one of FR4 ( $\alpha_T = 1.6 \cdot 10^{-5} \text{ 1/K}$ ), the PCB is shrinking around the silicon what leads to a thermal stress to the silicon [2].

*Direct cooling:* In the direct cooling the PCB is bypassed. Two stripes of a thermal pad, which conduct heat but are electrically isolating, are directly lying on opposing edges of the silicon. They are held in place by copper plates that are very gently pressing them on the silicon. These copper plates are also used for conducting heat from the pads to the cooled cooling structure. A disadvantage is that the pressure applied to the silicon can induce additional leakage current. The advantages are that the low heat conductivity of the PCB is not limiting the cooling and additionally the PCB does not necessarily have to be very cold, reducing the thermal stress to the silicon.

### 3.3.1 Indirect cooling

The indirect cooling works via heat conduction through the PCB. Since the shape of the PCB is not trivial (see figure 3.3) the simple formulas for thermal conductance 2.11 and thermal resistance 2.12 can't be used here. Therefore a simulation was made with Solid Works. The simulation uses the finite element method to solve the partial differential equation 2.7 universally describing heat conduction.

**finite element method** The finite element method is an approach to calculate an approximate solution for complicated differential equations. The continuous volume is represented in the computer by a discrete lattice. The user gives the computer a set of start parameters. Then the computer step by step calculates the interaction of adjacent points and changes the parameters. In case the problem has an equilibrium solution and the start parameters were chosen wisely, the parameters converge to the equilibrium solution.

The simulation only included heat conduction, a constant cooling liquid temperature ( $T_{liquid} = -12^{\circ}\text{C}$ ) and a volume heat source<sup>1</sup>  $P_{source}$  in the silicon. From the simulated equilibrium state the average silicon temperature  $T_{silicon}$  is obtained to calculate the temperature gradient between silicon and cooling liquid  $\Delta T = T_{liquid} - T_{silicon}$ . Since in the equilibrium state the power of the volume heat source equals the heat flux through the PCB, the thermal conductance can now be calculated using equation 2.11.

$$\sigma_Q = \frac{\Phi}{-\Delta T} = \frac{P_{source}}{T_{silicon} - T_{liquid}}$$



Figure 3.3: Cross-section of indirect cooling for a pion tracker detector. The cooling structure made of copper and the thermal pads (white) that are pinched between detector-PCB and cooling structure can be seen.

<sup>1</sup>The total power of the source is spread equally in the whole volume.

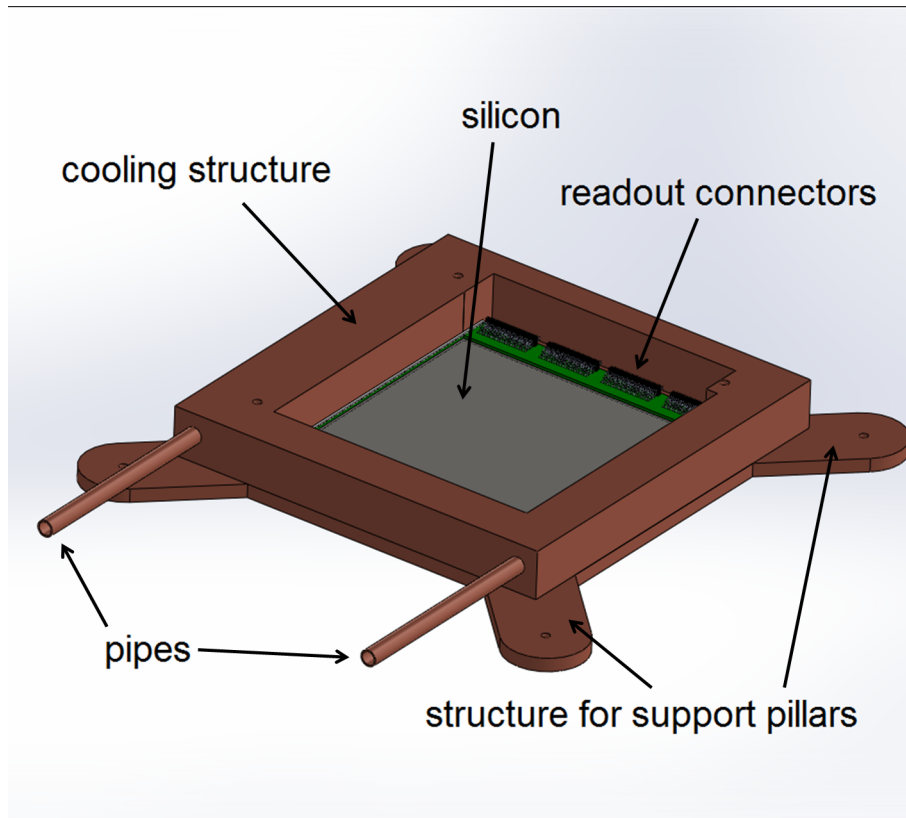


Figure 3.4: Indirect cooling for a pion tracker detector. The cooling structure is cooled by the cooling liquid. The heat from the silicon is transferred to the cooling structure by heat conduction via the PCB.

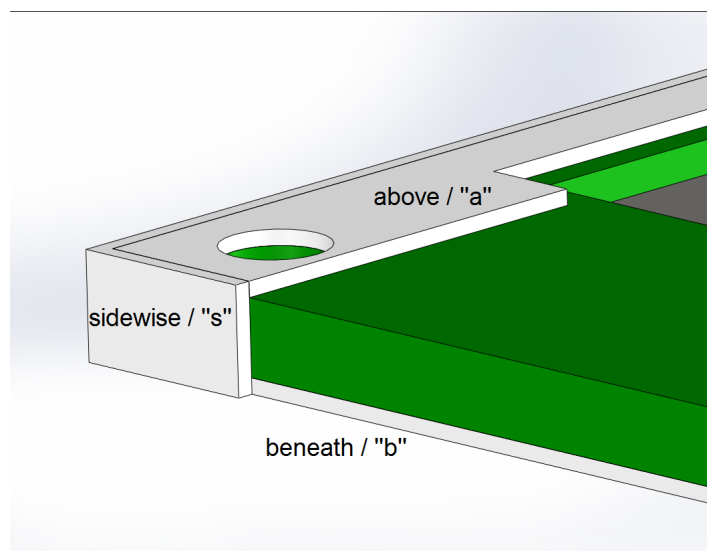


Figure 3.5: The thermal pads surrounding the PCB are shown. They isolate imprinted circuits on the PCB from the cooling structure.

Slightly different setups have been simulated:

- with and without the glue (KJR 9022E , thickness: 0.1 mm) between the edges of the silicon and the PCB, which the silicon is lying on
- with contact of the PCB to the copper cooling structure via a thermal pads (Keratherm®-Softtherm®, 86/600<sup>2</sup>) that are placed above and beneath ("a,b") or above, beneath and sidwise ("a,b,s") the PCB (see figure 3.5)

In both cases the thermal conductivity of the PCB made of FR4 was assumed to be  $\lambda = 0.27 \frac{\text{W}}{\text{m}\cdot\text{K}}$ .

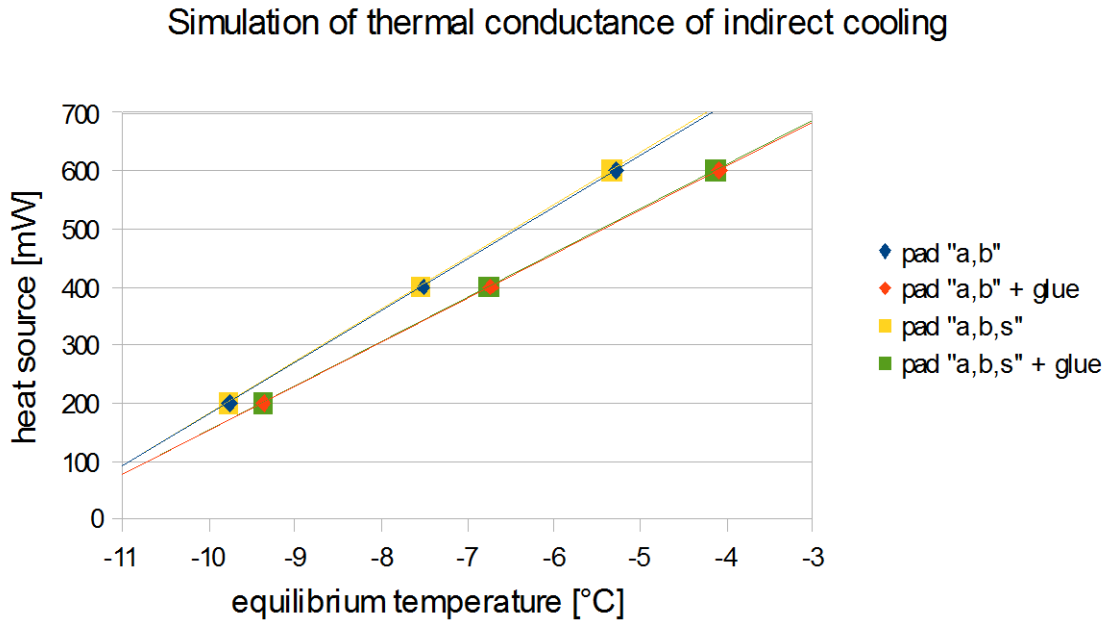


Figure 3.6: Results of the simulations of the different indirect cooling setups. The axes are switched in comparison to the usual arrangement so that the gradient of a linear fit corresponds to the thermal conductance.

The data in figure 3.6 can be fitted with a linear function. The gradient of the fits corresponds to the thermal conductance of the specific setup of the indirect cooling.

- pad "a,b":  $\sigma_Q = 89.29 \frac{\text{mW}}{\text{K}} \approx 90 \frac{\text{mW}}{\text{K}}$
- pad "a,b,s":  $\sigma_Q = 89.89 \frac{\text{mW}}{\text{K}} \approx 90 \frac{\text{mW}}{\text{K}}$
- pad "a,b" + glue:  $\sigma_Q = 75.76 \frac{\text{mW}}{\text{K}} \approx 75 \frac{\text{mW}}{\text{K}}$
- pad "a,b,s" + glue:  $\sigma_Q = 76.19 \frac{\text{mW}}{\text{K}} \approx 75 \frac{\text{mW}}{\text{K}}$

<sup>2</sup>Here the newer thermal pads were used, that were not available when the direct cooling prototype for SiAVio was built.

This shows that it does not make an important difference, if the PCB is in contact to the cooling structure over a thermal pad at its sides or not. On the other hand the glue between silicon and PCB has to be considered. So the thermal conductance of the indirect cooling for the pion tracker detector can be approximated with the thermal conductance of the simulation setup pad "a,b,s" + glue.

$$\sigma_{Q,PT}^{indirect} \approx 75 \frac{\text{mW}}{\text{K}}$$

### 3.3.2 Direct cooling

In the direct cooling the heat is conducted through the thermal-pads (Thermipad® TP 22600) and the copper plates, which are connected in series to each other (see figure 3.8).

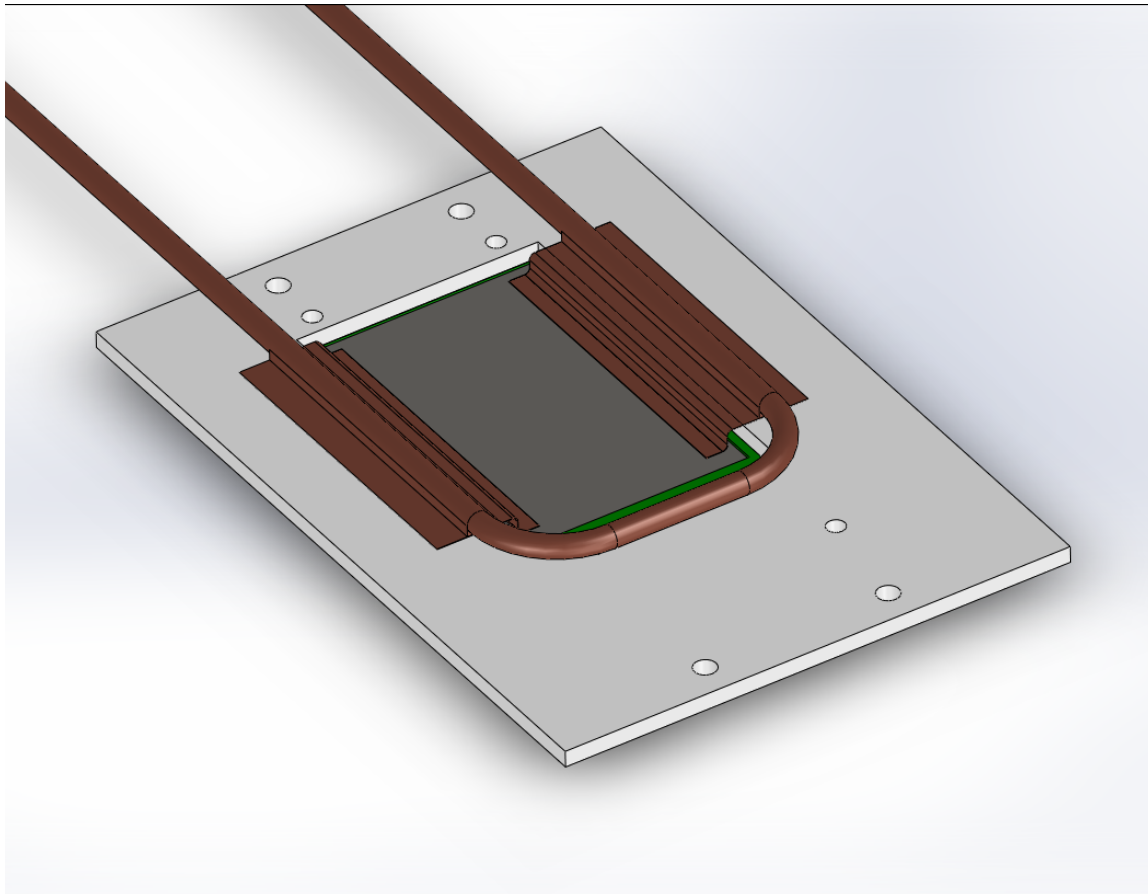


Figure 3.7: Direct cooling for SiAVio. The big plastic mounting structure and the cooling pipes can be seen.



Figure 3.8: Cross-section of direct cooling for SiAVio. The bent copper plates and the thermal pad (red) can be seen.

The thermal conductance of this cooling is calculated in following tables. Thermal transition resistances are not taken into account.

SiAVio	thermal pad	copper foil	total
distance $x$	0.5 mm	10 mm	-
cross sectional area $A$	$3 \times 50 \text{ mm}^2$	$0.1 \times 50 \text{ mm}^2$	-
thermal conductivity $\lambda$	$1 \frac{\text{W}}{\text{m}\cdot\text{K}}$	$400 \frac{\text{W}}{\text{m}\cdot\text{K}}$	-
thermal resistance $R_Q$	$3.33 \frac{\text{K}}{\text{W}}$	$5.00 \frac{\text{K}}{\text{W}}$	$4.17 \frac{\text{K}}{\text{W}}$
thermal conductivity $\sigma_Q^{\text{direct}}$	$0.30 \frac{\text{W}}{\text{K}}$	$0.20 \frac{\text{W}}{\text{K}}$	$0.24 \frac{\text{W}}{\text{K}}$

pion tracker	thermal pad	copper foil	total
distance $x$	0.5 mm	10 mm	-
cross sectional area $A$	$3 \times 90 \text{ mm}^2$	$0.1 \times 90 \text{ mm}^2$	-
thermal conductivity $\lambda$	$1 \frac{\text{W}}{\text{m}\cdot\text{K}}$	$400 \frac{\text{W}}{\text{m}\cdot\text{K}}$	-
thermal resistance $R_Q$	$1.85 \frac{\text{K}}{\text{W}}$	$2.78 \frac{\text{K}}{\text{W}}$	$2.32 \frac{\text{K}}{\text{W}}$
thermal conductivity $\sigma_Q^{\text{direct}}$	$0.54 \frac{\text{W}}{\text{K}}$	$0.36 \frac{\text{W}}{\text{K}}$	$0.43 \frac{\text{W}}{\text{K}}$

### 3.4 Technical data of the chiller

The heat coming from the different sources discussed in section 3.2 has to be dissipated. Since the goal is not only to maintain room temperature, but to cool the detector to beneath  $0^\circ\text{C}$  a cooling device is needed. The chiller that is used is the “CC-K6s” manufactured by HUBER KÄLTEMASCHINENBAU GMBH.

As a cooling liquid a water-propylenglycol mixture is used. The freezing point is dependent on the mixing ratio (see table 3.5). The mixing ratio that was used for the prototype tests is 60 vol% water, 40 vol% propylenglycol. With this mixture chiller temperatures of  $-16/ -17^\circ\text{C}$  could be maintained.

Temperature range	−25...200°C			
Temperature stability	±0.2°C			
Pump performance	27 l/min			
Maximum pump pressure	0.7 bar			
Fill volume	2.5 l			
Maximum tank volume	4,5 l			
Temperature of cooling liquid	20°C	0°C	−10°C	−20°C
maximum cooling power	260 W	210 W	150 W	50 W

Table 3.4: Technical data of the cooling device.

weight %	volume %	freezing point°C
0	0	0
20	19.4	-7.1
25	24.4	-9.6
30	29.4	-12.7
35	34.4	-16.5
40	39.4	-21.1
45	44.4	-26.7
50	49.4	-33.5

Table 3.5: Freezing point of a water-propylenglycol mixture dependent on the propylenglycol concentration.



---

## 4 Measurements with first prototype

The measurements with the first SiAVio prototype have been made to investigate how it performs and what problems might occur. To have an experimental feedback is very important to identify practical problems early so that they can be included in the development of the next cooling design.

The first measurements with the SiAVio prototype have been performed under vacuum condition. This is necessary because cooling below  $0^{\circ}\text{C}$  is causing humidity to condense on the detector and water could corrode the printed circuits. So vacuum is not only needed in the final beam-line but also for the cooling tests. Nevertheless the vacuum for the cooling tests ( $\sim 10^{-3}$  mbar) was much weaker than the vacuum needed in the final setup, which is located in the beam-line ( $\sim 10^{-8}$  mbar). Besides that the operation in an vacuum environment eliminates the heating due to convection in air, which is already the case at a pressure of  $\sim 10^{-3}$  mbar.

The measurements have been made with the following procedure:

1. precooling for several hours to  $-16^{\circ}\text{C}$  (over night)
2. raising temperature by steps of  $1^{\circ}\text{C}$  up to  $-5^{\circ}\text{C}$
3. 5 minute break after changing temperature before reading out temperature sensors

For measuring the temperature four “one-Wire” sensors were attached to the cooling pipe at different locations with a heat conducting glue (NEE-001) and a “PT-100” sensor was slightly pressed against the silicon surface. To protect the surface from scratches a thermal pad was placed between the PT 100 and the silicon.

### 4.1 Temperature curves

Temperature curves have been measured for the following setups:

- SiAVio prototype with readout cables attached to the detector and no voltage applied to the silicon
- SiAVio prototype with no readout cables attached to the detector
- SiAVio prototype with readout cables attached to the detector and a voltage of 250 V applied to the silicon

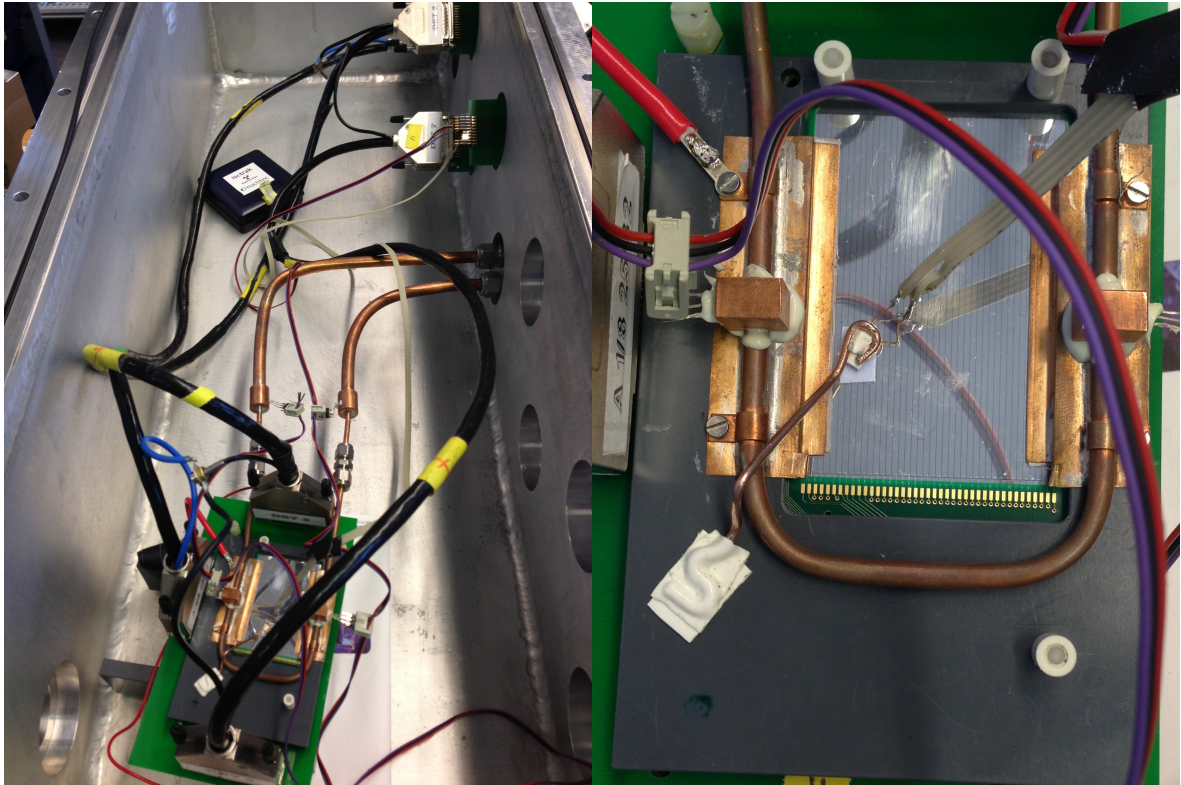


Figure 4.1: Pictures of the prototype before the tests. Left: The vacuum chamber, readout cables and cooling liquid pipe can be seen. Right: Direct cooling system and different temperature sensors can be seen.

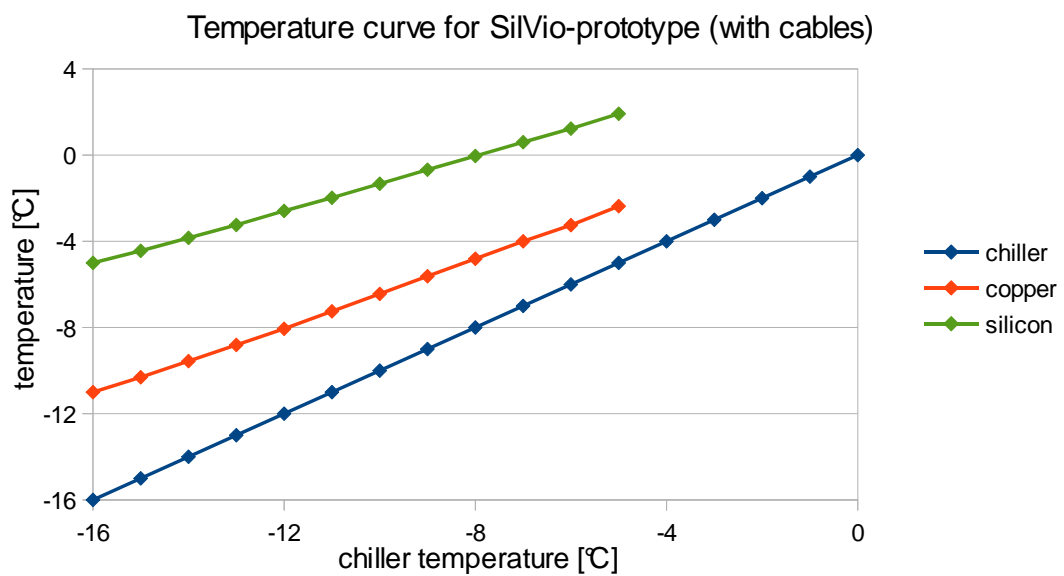


Figure 4.2: Temperature of the copper mounting and the silicon for different chiller temperatures. The setup included readout cables. No voltage was applied to the silicon.

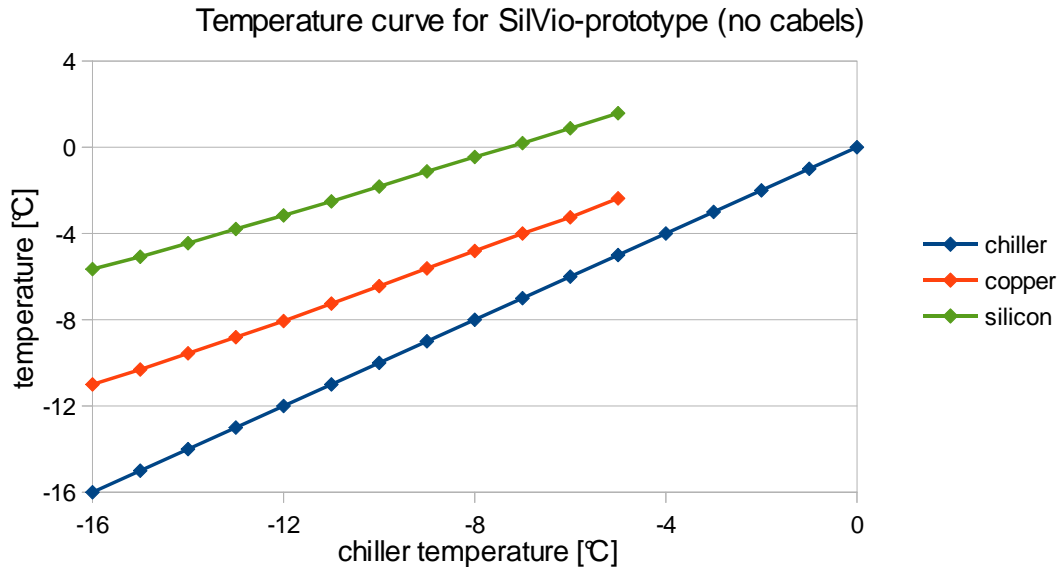


Figure 4.3: Temperature of the copper mounting and the silicon for different chiller temperatures. In the setup the readout cables were not connected to the detector. No voltage was applied to the silicon.

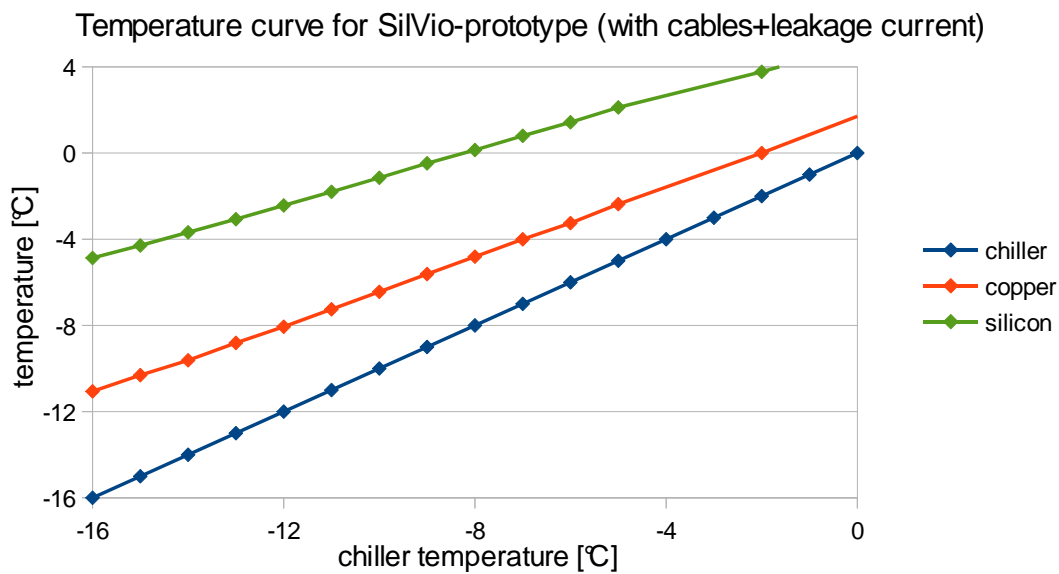


Figure 4.4: Temperature of the copper mounting and the silicon for different chiller temperatures. The setup included readout cables. Additionally a voltage of 250 V was applied to the silicon and therefore a leakage current was flowing ( $\sim 2.5 \mu\text{A}$ ).

## 4.2 Analysis of temperature gradients

Since the different measurements only differ slightly just the temperature gradients of the setup with readout cables attached to the detector but no voltage applied is shown and discussed.

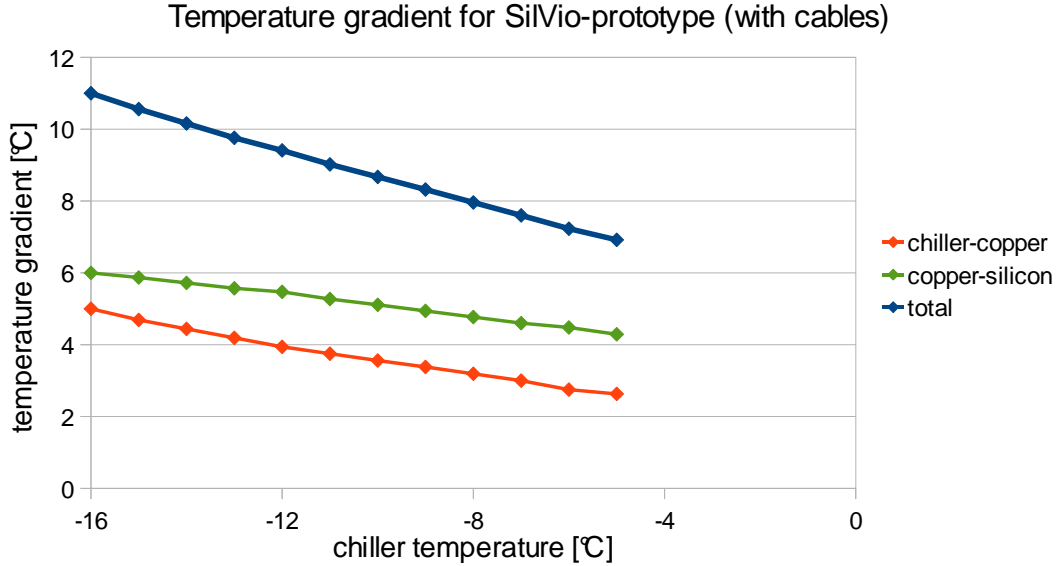


Figure 4.5: Temperature gradient between chiller-copper and copper-silicon for different chiller temperatures. The setup included readout cables. No voltage was applied to the silicon.

At  $-16^{\circ}\text{C}$  chiller temperature the temperature gradient caused by cooling liquid flow is  $\Delta T_{flow} = 5^{\circ}\text{C}$  and the temperature gradient caused by heat conduction is  $\Delta T_{conduct} = 6^{\circ}\text{C}$ . This shows that for improving the cooling system the cooling itself as well as the transport of the cooling fluid have to be improved.

With the thermal conductance of the direct cooling for SiLVio ( $\sigma_{Q,Sil}^{direct} = 240 \text{ mW/K}$ , see 3.3.2) the total heating power to the silicon is approximately 1400 mW. This is much more than the expected heating power of  $P_{Sil}^{AR} = 70\text{--}110 \text{ mW}$ . Only the heating power of heat radiation to the mounting structure  $P_{Sil,mount}^{AR}$  is in the same order of magnitude. A possible explanation for the high temperature difference  $\Delta T_{conduct}$  is that the heating to the mounting structure by heat radiation is not transferred to the cooling liquid, due to a bad thermal conductance between PCB and copper pipe caused by the plastic mounting structure in between. So the PCB heats up and becomes warmer than the silicon. Then heat is conducted from the PCB to the silicon, which additionally has to be conducted through the direct cooling.

### 4.3 Influence of readout cables

The influence of the readout cables can be analysed by comparing the temperature curves for the setup with and without readout cables. The difference  $\Delta T_{cables} = T_{silicon,with\ cables} - T_{silicon,without\ cables}$  can be seen in figure 4.6.

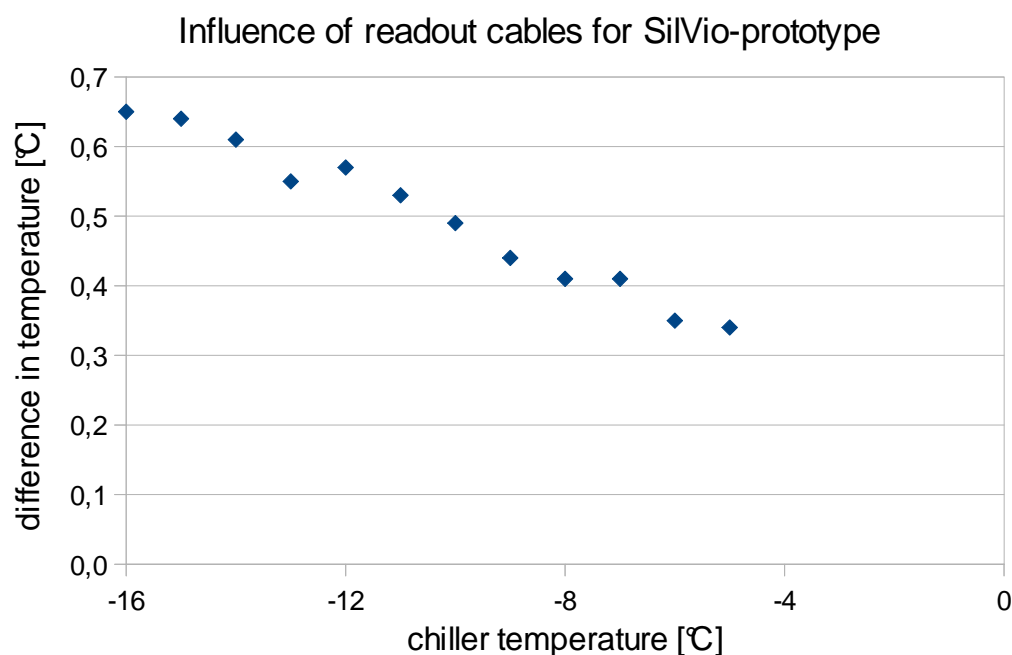


Figure 4.6: Difference in the silicon temperature for the measurements with and without readout cables.

The difference  $\Delta T_{cables}$  is positive, so the readout cables conduct additional heat to the detector. Moreover  $\Delta T_{cables}$  is decreasing with higher chiller temperature. This can be explained by the fact that the temperature gradient between detector and vacuum chamber is decreasing, leading to a smaller heat flux through the readout cables.

With the thermal conductance of the direct cooling for SiVio ( $\sigma_{Q,Sil}^{direct} = 240 \text{ mW/K}$ , see 3.3.2) and the estimated heating power of the cables to the connectors ( $P_{Sil}^{RC} = 115\text{--}220 \text{ mW}$ , see 3.2) the expected influence should be between  $0.5\text{--}0.9^\circ\text{C}$  or less, depending on how good the heat is transferred from the connectors to the silicon. The expected influence matches the measured influence. This suggests that the heat is conducted from the connectors to the silicon very well.

## 4.4 Influence of leakage current

The influence of the leakage current as a heat source can be analysed by comparing the temperature curves for the setup with readout cables and voltage applied to the silicon to the temperature curve for the setup with readout cables but without voltage applied to the silicon. The difference  $\Delta T_{leakage\ current} = T_{silicon,with\ cables+leakage\ current} - T_{silicon,with\ cables}$  can be seen in figure 4.7.

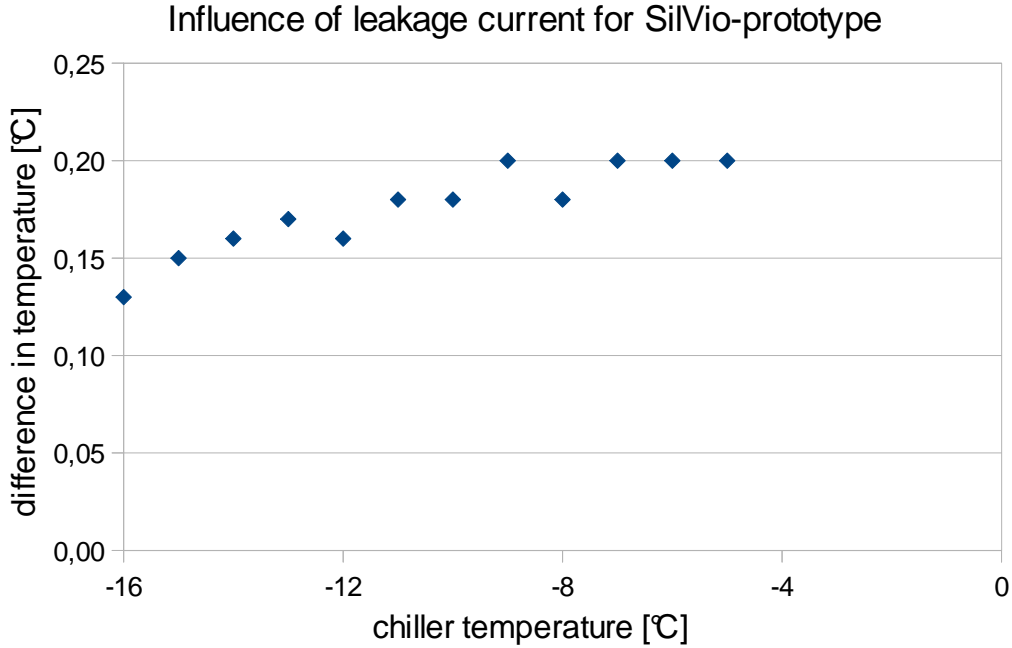


Figure 4.7: Difference in the silicon temperature for the measurements with and without leakage current.

With the thermal conductance of the direct cooling for SiAVio ( $\sigma_{Q,direct,Sil} = 240 \text{ mW/K}$ , see 3.3.2) and the estimated heating power of the leakage current ( $P_{Sil}^{LC} = 625 \mu\text{W}$ , see 3.2) the expected influence should be less than  $0.01^\circ\text{C}$ . Since the temperature stability of our chiller is approximately  $\pm 0.2^\circ\text{C}$  and the room temperature outside the chamber also varies slightly the much higher temperature difference could be just a temperature fluctuation. If the temperature difference is not a fluctuation the heat generated by the leakage current should be in the order of  $P_{current,Sil} \approx 40 \text{ mW}$ . Considering that no reason for such a high heating power could be found, it is assumed that the difference in temperature is a fluctuation.

## 5 Evaluation of improvement potential

To achieve an efficient cooling the temperature gradient between chiller and detector has to be minimised. This temperature gradient can be allocated to two different temperature gradients:

- First the gradient between chiller and cooling structure:  

$$\Delta T_{flow} = T_{mount} - T_{chiller}$$
- Second the gradient between cooling structure and silicon detector:  

$$\Delta T_{conduct} = T_{silicon} - T_{mount}$$

These two cases have been separated, because of the different types of heat transport. Between the chiller and the copper the flow of the cooling liquid is transporting the heat. Between the copper and the silicon heat is only transported via heat conduction in solid materials. Therefore the approaches to decrease the temperature gradients are mostly different. In chapter 4 it could be seen that both temperature gradients have roughly the same size and therefore have to be reduced both.

### 5.1 Reducing temperature gradient due to heat conduction

$$\Delta T_{conduct} = -\frac{\Phi}{\sigma_Q}$$

This equation can be obtained from equation 2.11. It shows that there are two ways to reduce the temperature gradient due to heat conduction. Either increase the thermal conductance or decrease the heat flux. Since in an equilibrium state the heat flux equals the total heating power to the silicon, decreasing heat flux implies reducing the heat sources' power.

#### 5.1.1 Direct cooling

The thermal conductance of the direct cooling was limited due to the thin copper foil (0.1 mm). The foil was chosen so thin because it needs to be very flexible to limit the pressure on the silicon. Nevertheless the rigidity of the foil was high enough to

influence the leakage current. The silicon is so sensible that even the small pressure applied by the foil was too much. To improve the thermal conductance a new design was developed. The goal was to replace the copper foil with a copper sheet to maximise thermal conductance. On the other hand the copper sheet is inelastic. So the cooling structure was attached to the mounting structure with pillars, which makes it possible to place washers between the pillars and the cooling structure (see fig. 5.2). With the thickness of the washers the pressure on the silicon can be adjusted. The design of a direct cooling system for the pion tracker detector can be seen in figure 5.1.

Additionally another manufacturer of heat conducting foils was found. The KERAFOL KERAMISCHE FOLIEN GMBH produces a variety of heat conducting foils. The “Keratherm®-Softtherm®, 86/600” with a thermal conductivity of  $6 \text{ W/m}\cdot\text{K}$  is a good improvement to the previously used foil.

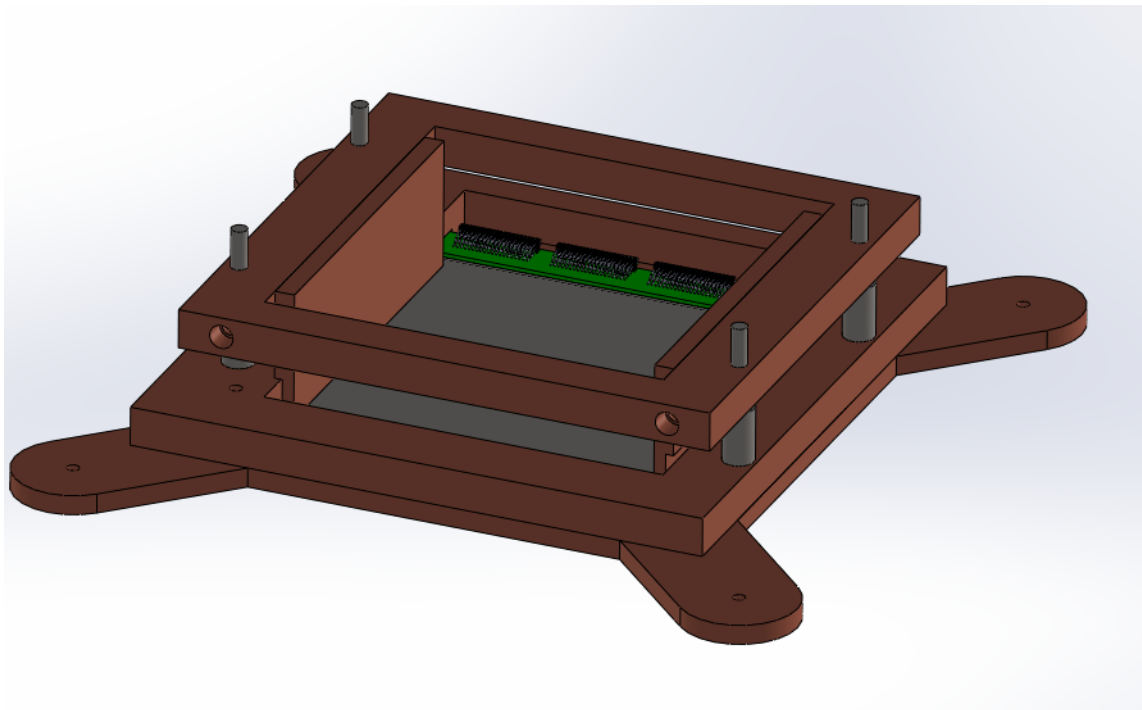


Figure 5.1: New design of a direct cooling for the pion tracker detector. The thin copper foils were replaced by copper sheets. The pressure on the silicon can be adjusted by using different washers.

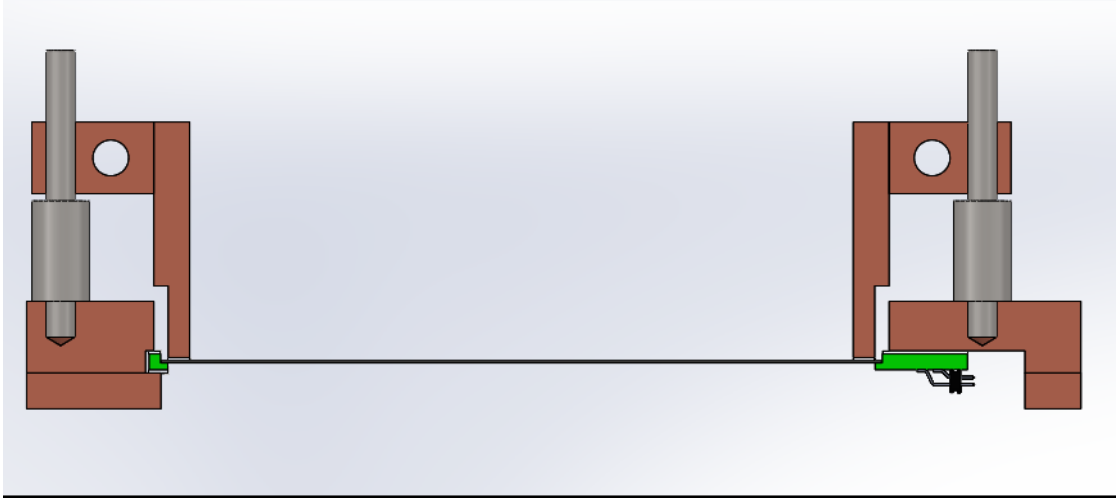


Figure 5.2: Cross-section of improved direct cooling for pion tracker, the copper sheets and the thermal pad (white) can be seen.

The thermal conductance of this new design is calculated in following tables. Thermal transition resistances are not taken into account.

SiAVio	thermal pad	lower copper sheet	upper copper sheet	total
distance $x$	0.5 mm	10 mm	20 mm	-
cross sectional area $A$	$3 \times 50 \text{ mm}^2$	$3 \times 50 \text{ mm}^2$	$5 \times 50 \text{ mm}^2$	-
thermal conductivity $\lambda$	$6 \frac{\text{W}}{\text{m}\cdot\text{K}}$	$400 \frac{\text{W}}{\text{m}\cdot\text{K}}$	$400 \frac{\text{W}}{\text{m}\cdot\text{K}}$	-
thermal resistance $R_Q$	$0.55 \frac{\text{K}}{\text{W}}$	$0.17 \frac{\text{K}}{\text{W}}$	$0.20 \frac{\text{K}}{\text{W}}$	$0.46 \frac{\text{K}}{\text{W}}$
thermal conductivity $\sigma_Q^{\text{direct}}$	$1.80 \frac{\text{W}}{\text{K}}$	$6.00 \frac{\text{W}}{\text{K}}$	$5.00 \frac{\text{W}}{\text{K}}$	$2.17 \frac{\text{W}}{\text{K}}$

pion tracker	thermal pad	lower copper sheet	upper copper sheet	total
distance $x$	0.5 mm	10 mm	20 mm	-
cross sectional area $A$	$3 \times 90 \text{ mm}^2$	$3 \times 90 \text{ mm}^2$	$5 \times 90 \text{ mm}^2$	-
thermal conductivity $\lambda$	$6 \frac{\text{W}}{\text{m}\cdot\text{K}}$	$400 \frac{\text{W}}{\text{m}\cdot\text{K}}$	$400 \frac{\text{W}}{\text{m}\cdot\text{K}}$	-
thermal resistance $R_Q$	$0.31 \frac{\text{K}}{\text{W}}$	$0.09 \frac{\text{K}}{\text{W}}$	$0.11 \frac{\text{K}}{\text{W}}$	$0.26 \frac{\text{K}}{\text{W}}$
thermal conductivity $\sigma_Q^{\text{direct}}$	$3.24 \frac{\text{W}}{\text{K}}$	$10.80 \frac{\text{W}}{\text{K}}$	$9.00 \frac{\text{W}}{\text{K}}$	$3.92 \frac{\text{W}}{\text{K}}$

### 5.1.2 Indirect cooling

In 5.1.2 it became clear, that a indirect cooling is very limited in terms of thermal conductance. A way of improving the temperature gradient between detector and cooling structure is to decrease the total of the heat sources' power. The different heat sources were already discussed in 3.2. Here different approaches to decrease the heating power and their effectiveness will be presented.

Reducing heating from ambient radiation:

- shielding "Fridge"
- reflecting Foil

Reducing heat conduction through readout cables:

- cooling readout cables

#### Shielding "Fridge":

The heat radiation could be reduced by mounting a cooled copper tube around the detector that shields the incoming heat radiation ( $T = 20^{\circ}\text{C}$ ) from the chamber and vacuum pipe. This kind of setup will be referred to as fridge.

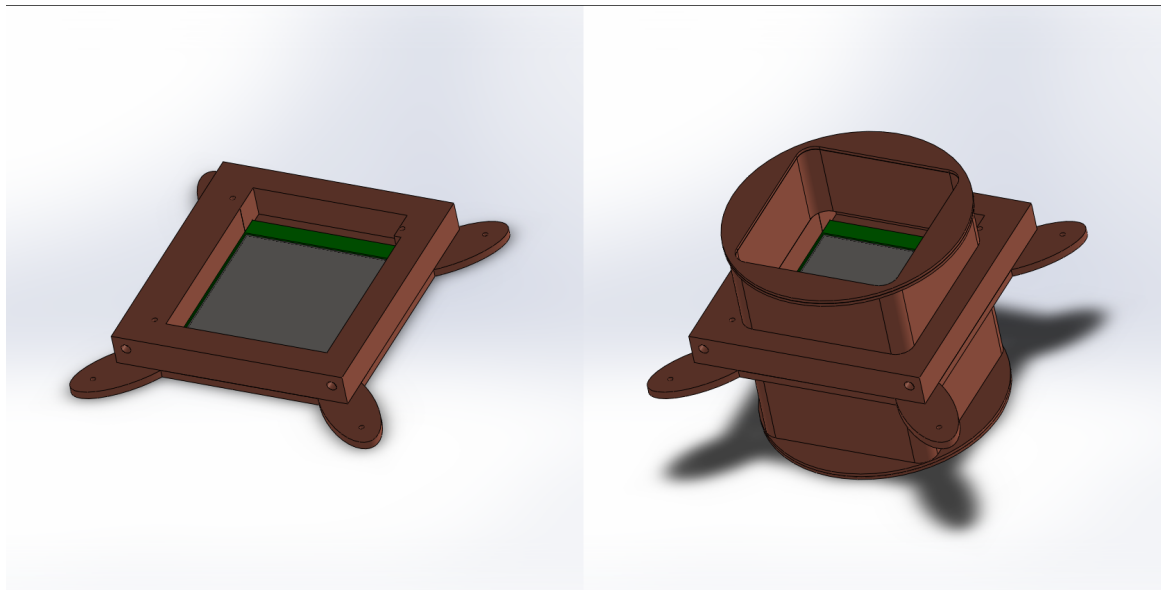


Figure 5.3: Indirect cooling for a pion tracker detector without fridge (left) and with fridge (right). The fridge gets cooled via the cooling structure and is shielding part of the incoming heat radiation.

To estimate the effect of a fridge it is important to know the covered solid angle seen from the silicon. The open solid angle for a certain point on the silicon can be

calculated using the Oosterom-Strackee algorithm. To get the average open solid angle seen from the silicon, the detector surface was split into  $1000 \times 1000$  identical squares. For these the open solid angle was calculated for their center (see figure 5.4). The arithmetic mean over all squares is shown in figure 5.5. The programming code of the root macro used is in the appendix.

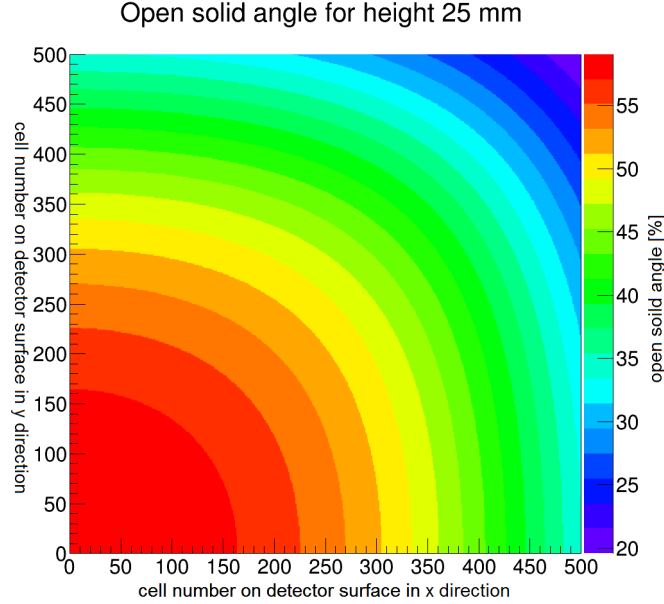


Figure 5.4: The figure shows 1/4 of the detector. (0,0) is the center and (500,500) is one edge. The colour represents the open solid angle in percent seen from the specific point for a  $100 \times 100$  mm detector and a fridge height of 25 mm.

The fridge is directly mounted on the cooling structure and as a result its temperature is similar to the one of the cooling structure. So the temperature of the fridge is lower than the detector temperature. Therefore the exchange of heat radiation between silicon and the interior of the fridge does not lead to an energy flux to the silicon. In fact there is even a small energy flux from the silicon to the fridge, but since it is the goal to minimise the temperature gradient between silicon and cooling structure, the energy flux is neglected.

The height a fridge is limited due to the vacuum chamber to 45 mm. In conjunction with a reflecting foil a fridge height of 20 to 30 mm should be sufficient to strongly reduce the heating by radiation. With this height the fridge covers 50–60% of the solid angle and the foil reflects a big share of the other 40–50%. Additionally problems with the spacing inside the vacuum chamber are prevented.

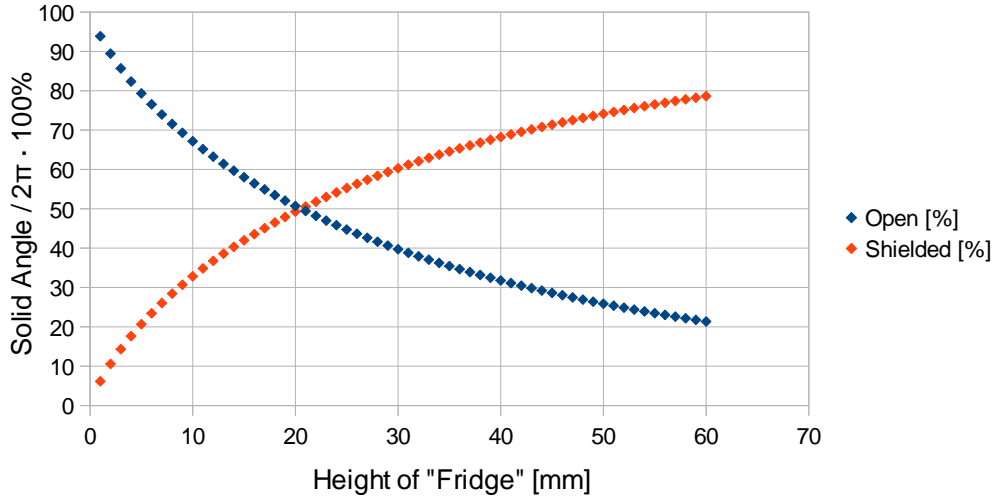


Figure 5.5: The graph shows the share of the solid angle that is shielded by the fridge: The detector has a surface of  $100 \times 100 \text{ mm}^2$ , which was also used as the internal dimension of the fridge. The height is measured from the surface of the detector to the upper edges of the fridge.

### Reflecting foil:

A thin foil placed before and after the detector in the beam line could reflect the incoming heat radiation. Since the particles of the beam may not be influenced, the thickness of the foil has to be chosen carefully. An approach to set a limit for the foil is to compare area density  $\rho_A$  of the silicon detector with the one of a foil, since the interaction of high energy particles is roughly proportional to the density traversed.

$$\rho_A = \frac{m}{A} = \frac{\rho \cdot V}{A} = \frac{\rho \cdot A \cdot d}{A} = \rho \cdot d \quad (5.1)$$

The silicon detector has a thickness of  $d_{detector} = 300 \mu\text{m}$  and the density of silicon is  $\rho_{silicon} = 2.34 \text{ g/cm}^3$ . This gives an area density of  $\rho_{A,detector} = 70 \text{ mg/cm}^2$ . As limit was defined, that the area density of the foils should not exceed 1% of the detectors area density. Since there are two foils per detector the maximum area density for the reflecting foil is  $\rho_{A,foil,max} = 350 \mu\text{g/cm}^2$ .

For reflecting heat radiation, which is mainly in the infrared spectrum, metals are the perfect material due to their high charge carrier density. Very thin pure metal foils rip very easily based on the low flexibility. Therefore a flexible synthetic mylar foil coated with a thin metal layer is a good solution. The mylar, which is a polyester film, has a good stability and the metal layer reflects heat radiation.

### Cooling of the readout cables:

The idea is to press the readout cables, which are connected to the connectors on the PCB, against the cooling structure (see figure 3.4 for picture of the cooling structure). This can be done by a metal bar, which is lying on the readout cables and screwed to the cooling structure at both ends. Like this the readout cables are cooled at the point of contact. So the temperature gradient in the part of the cables going to the detector is smaller and the heat flux to the silicon is reduced. But on the other hand there is a heat flux to the cooling structure, which is tolerated because it can be transferred to the cooling liquid more easily. The cooling of the readout cables more or less redirects the heat flux from the silicon to the cooling structure.

Additionally the effectiveness of cooling the readout cables in the pion tracker setup will be estimated. To be able to do this the complex geometry has to be reduced to 4 idealised points each representing one part of the setup.

**chamber** This point reflects the vacuum chamber. It is constantly at  $20^{\circ}\text{C}$  (room temperature).

**cooling structure** The cooling structure is given a constant temperature of  $-15^{\circ}\text{C}$ .

**silicon** The silicon is given a constant temperature of  $-10^{\circ}\text{C}$ .

**contact point** The contact point reflects the copper stripes in the readout cables at the point where the cables are pressed to the cooling structure. Its temperature is variable and will be calculated later. Furthermore the contact point is the only point that has a connection to each of the other points.

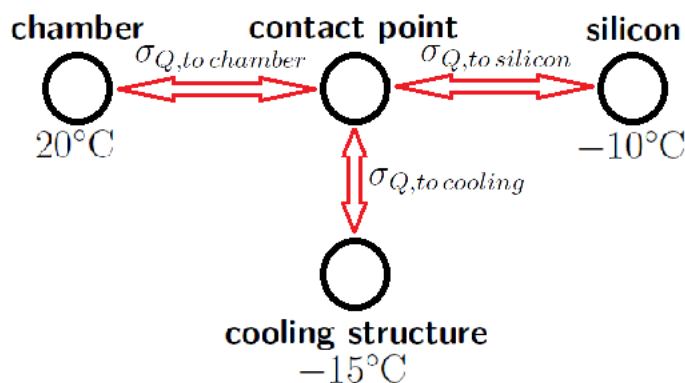


Figure 5.6: Sketch of the 4 points, which represent the setup in a simplified form. Additionally the connections that conduct heat between the points are shown. Since the setup is in vacuum only those points with a mechanical connection exchange heat (heat radiation is neglected in this calculation).

To calculate the heat flux from the contact point to each of the other points the thermal conductance of the connections has to be calculated. The readout cable is connecting the chamber to the contact point and the contact point to the silicon. The properties of the readout cables were discussed in chapter 3.2. The length of the cable is now split up to both connections. Following lengths will be used  $l_{\text{contact-silicon}} = 3$  cm and  $l_{\text{contact-chamber}} = 7$  cm. The connection from the contact point to the cooling structure is caused by the kapton sheath. It is assumed that the cable is pressed to the cooling structure at its full width and at a length of 0.5 cm. In the calculation properties with an uncertainty were chose in a way that the efficiency of the readout cable cooling is minimal. So the effect of the readout cable cooling should be at least what is estimated.

connection to:	cooling structure (1 cable)	chamber (1 cable)	silicon (1 cables)
distance $x$	$90 \mu\text{m}$	$70 \text{ mm}$	$30 \text{ mm}$
cross sectional area $A$	$5 \times 20 \text{ mm}^2$	$0.32 \text{ mm}^2$	$0.32 \text{ mm}^2$
thermal conductivity $\lambda$	$0.12 \frac{\text{W}}{\text{m}\cdot\text{K}}$	$400 \frac{\text{W}}{\text{m}\cdot\text{K}}$	$400 \frac{\text{W}}{\text{m}\cdot\text{K}}$
thermal conductance $\sigma_Q$	$133.33 \frac{\text{mW}}{\text{K}}$	$1.83 \frac{\text{mW}}{\text{K}}$	$4.27 \frac{\text{mW}}{\text{K}}$

In equilibrium the total heat flux to the contact point is zero. This is now used to calculate its temperature.

$$(T_{\text{contact}} - T_{\text{chamber}}) \cdot \sigma_{Q,\text{to chamber}} + (T_{\text{contact}} - T_{\text{silicon}}) \cdot \sigma_{Q,\text{to silicon}} + (T_{\text{contact}} - T_{\text{cooling}}) \cdot \sigma_{Q,\text{to cooling}} = 0$$

$$T_{\text{contact}} = \frac{T_{\text{chamber}} \cdot \sigma_{Q,\text{to chamber}} + T_{\text{silicon}} \cdot \sigma_{Q,\text{to silicon}} + T_{\text{cooling}} \cdot \sigma_{Q,\text{to cooling}}}{\sigma_{Q,\text{to chamber}} + \sigma_{Q,\text{to silicon}} + \sigma_{Q,\text{to cooling}}} = -14.4^\circ\text{C}$$

The high conductivity to the cooling structure keeps the temperature very low. Since it is even lower than the silicon temperature we now even have an additional heat flux from the silicon to the mounting. The heat flux to the mounting and from the silicon are now calculated taking in account all 8 cables.

$$P_{PT,\text{to cooling}} = 8 \cdot \sigma_{Q,\text{to cooling}} \cdot (T_{\text{contact}} - T_{\text{cooling}}) = 640 \text{ mW}$$

$$P_{PT,\text{to silicon}} = 8 \cdot \sigma_{Q,\text{to silicon}} \cdot (T_{\text{contact}} - T_{\text{silicon}}) = -150 \text{ mW}$$

## 5.2 Reducing temperature gradient due to cooling liquid flow

The temperature gradient between the chiller and the cooling structure depends on the heat flux through the isolation of the pipe going to the vacuum chamber. The heat flux can be calculated with equation 2.11 and 2.14.

$$\Delta T_{flow} \propto \Phi = \sigma_Q \cdot (-\Delta T) = (T_{chiller} - T_{room}) \cdot 2\pi \cdot \lambda \cdot l_{pipe} \cdot \frac{1}{\ln\left(\frac{r_{out}}{r_{in}}\right)}$$

Therefore the length  $l_{pipe}$  of the pipe going to the vacuum chamber should be as short as possible. The ratio  $\frac{r_{out}}{r_{in}}$  of the isolation should be big and the thermal conductivity  $\lambda$  of the isolation material small.

A common material for isolation is synthetic caoutchouc with a heat conductivity of  $\lambda = 0.036 \text{ W/m}\cdot\text{K}$ . There are caoutchouc isolations available for purchase for 12 mm and 15 mm pipes with thicknesses of 6 mm, 10 mm and 20 mm. In the prototype tests a caoutchouc isolation for a 15 mm pipe with a thickness of 10 mm was used.

By replacing the isolation with a 20 mm isolation the heat flux from the 20°C room to the approximately  $-17^\circ\text{C}$  cooling fluid per meter pipe could be reduced from 9.9 to 6.4 W.

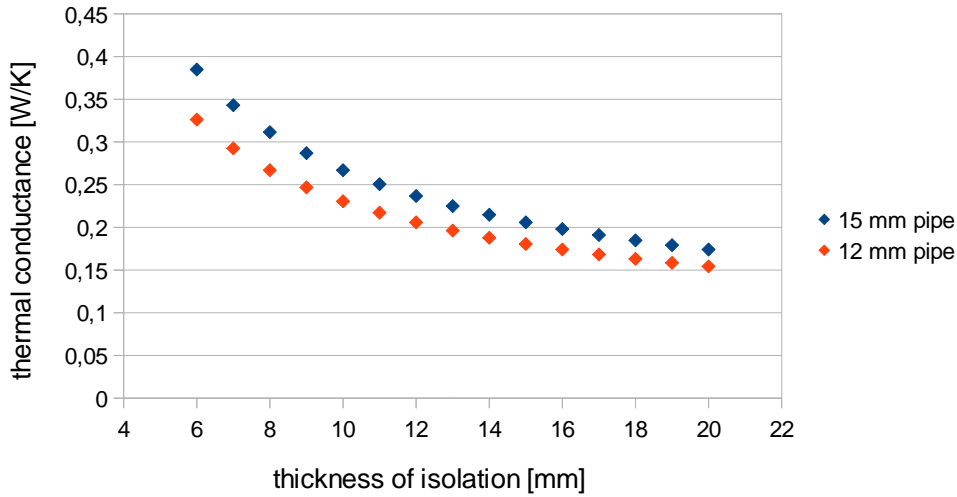


Figure 5.7: Thermal conductance between inside and outside of a one meter pipe dependent on the thickness of the caoutchouc isolation ( $\lambda = 0.036 \text{ W/m}\cdot\text{K}$ ).

Additionally the temperature gradient between the chiller and the cooling structure depends on the cooling liquid flow. With a higher flow the heat flux through the isolation is spread to more cooling liquid. Therefore the temperature of the cooling liquid increases less.

The flow through a pipe depends on the inner diameter  $d_{pipe}$  and the length  $l_{pipe}$ .

$$Q \propto \frac{1}{l_{pipe}} \cdot d_{pipe}^4$$

with volume flow  $Q$ .

Since the dependence on the inner diameter is so strong, the cooling liquid circuit should have no narrowings. The pipe outside the vacuum chamber is quite thick

compared to those inside the chamber. So the length  $l_{pipe}$  outside the vacuum chamber should be kept short mostly from lowering the heat flux to the cooling fluid and not primarily to increase the volume flow. To maximise the volume flow  $Q$  the most important thing is to connect the cooling system to the feedthroughs in the chamber with pipes that are not thinner than the pipes in the cooling system. Like this there are no narrowings in the cooling liquid circuit. Here it has to be said that in both prototype setups that were surveyed in chapter 4 and 6 there were narrow pipes in the cooling liquid circuit. The reason for that is that they can be bent more easily, which makes it possible to connect the pipes without having to wait for customised pipes to be made. Under the assumption of laminar flow the volume flow can be calculated using the Hagen-Poiseuille equation. The result is that the flow in a cooling liquid circuit without narrowings, which requires customised pipes, is 3 to 4 times higher than the one in the prototype setups.

## 6 Experimental validation

The measurements with the newly build indirect cooling prototype for an mechanical sample <sup>1</sup> of the pion tracker detector have been carried out to check the basic performance of an indirect cooling. Additionally different ways of reducing heat power discussed in chapter 5.1.2 were tested and their performance was compared to the simulated effect.

The experiments with the pion tracker prototype have been made in the same vacuum chamber that was used for the tests of the SiAVio prototype (see left picture in figure 4.1). The vacuum is needed to remove humidity that would condense on the detector and to suppress the effect of heating through natural convection in the air.

The measurements have been made with the following procedure:

1. precooling for several hours to  $-17^{\circ}\text{C}$  (over night)
2. raising temperature by steps of  $2^{\circ}\text{C}$  up to  $13^{\circ}\text{C}$
3. 13 minute break after changing temperature before reading out temperature sensors

In order to measure the temperature four “one-Wire” sensors were glued to the following places with a heat conducting glue (NEE-001):

- into the plastic cooling tube shortly before the vacuum chamber entrance (“tube”)
- to the copper cooling pipe before the detector mounting (“pipe in”)
- to the copper cooling pipe after the detector mounting (“pipe out”)
- to the detector cooling structure (“copper”)

For measuring the detector temperature a “PT-100” sensor was slightly pressed against the silicon surface.

---

<sup>1</sup>The mechanical sample can't be read out, but besides that all parts are identical to those of a working detector

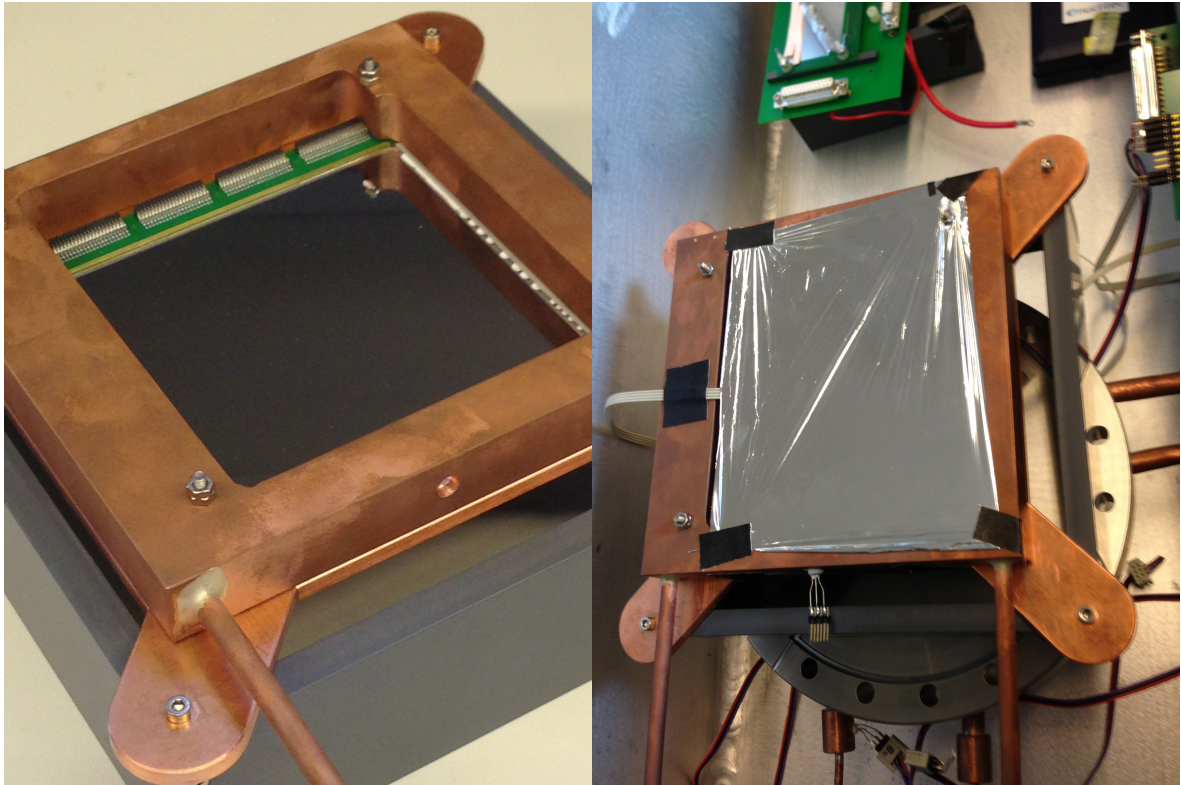


Figure 6.1: Pictures of the experimental setup. Left: The indirect cooling with the mechanical sample of the pion tracker detector. Right: Indirect cooling system in test vacuum chamber with reflecting mylar foil (thickness  $1.5\text{--}2\ \mu\text{m}$ , weight  $252\ \mu\text{g}/\text{cm}^2$  ).

## 6.1 Temperature curves

Temperature curves have been measured for the following setups:

- PT prototype
- PT prototype with reflecting mylar foil (thickness  $1.5\text{--}2\ \mu\text{m}$ , weight  $252\ \frac{\mu\text{g}}{\text{cm}^2}$  )

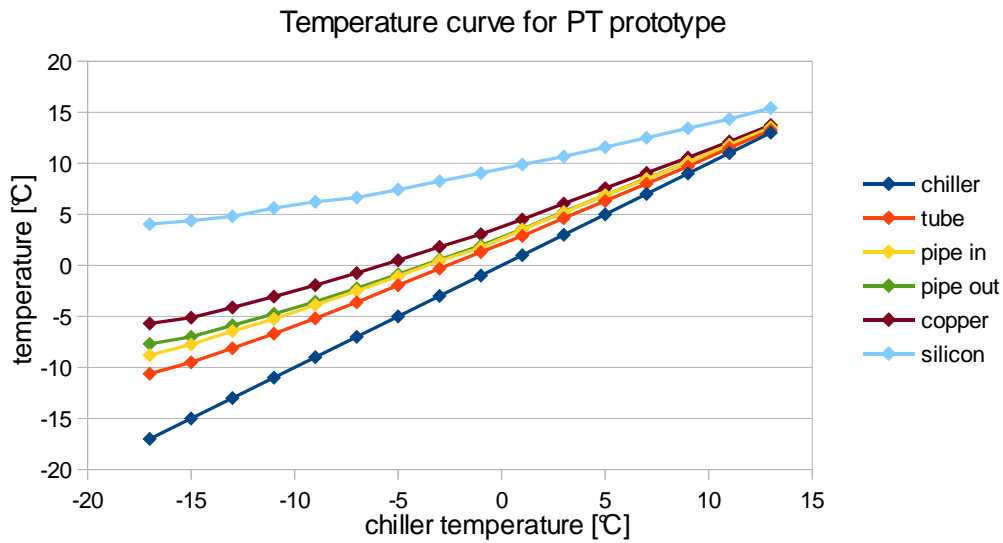


Figure 6.2: Temperature curves for different chiller temperatures. The setup included only the cooling structure of the indirect cooling (see left picture in figure 6.1).

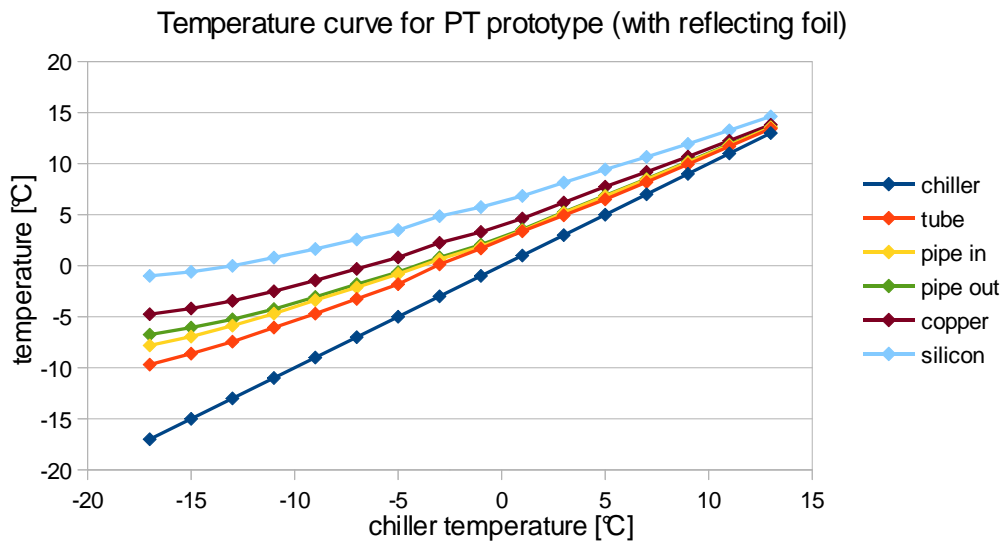


Figure 6.3: Temperature curves for different chiller temperatures. The setup included the cooling structure with the detector openings covered with a reflecting mylar foil (thickness  $1.5\text{--}2\ \mu\text{m}$ , weight  $252\ \mu\text{g}/\text{cm}^2$ ) (see right picture in figure 6.1).

## 6.2 Analysis of temperature gradients

Here the temperature gradients of the setup without mylar foil will be discussed. For this purpose the mean value of the temperatures "pipe in" and "pipe out" is taken. The newly gained value is called "pipe" temperature and should reflect the temperature of the cooling liquid inside the cooling structure. The influence of the mylar is analysed in the next section.

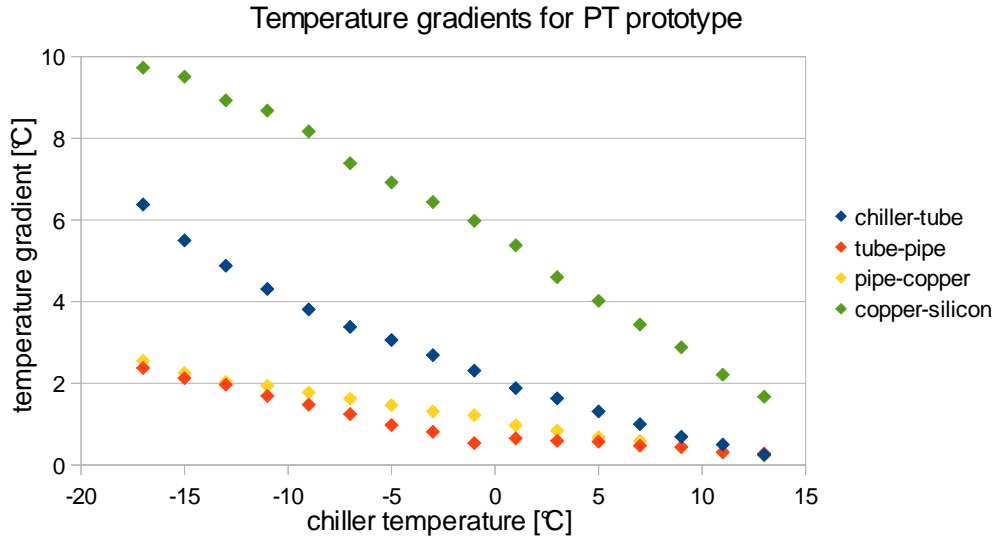


Figure 6.4: Temperature gradient between chiller-tube, tube pipe, pipe copper and copper-silicon for different chiller temperatures.

At  $-17^{\circ}\text{C}$  chiller temperature the temperature gradient caused by cooling liquid flow is  $\Delta T_{flow} = 11^{\circ}\text{C}$  and the temperature gradient caused by heat conduction is  $\Delta T_{conduct} = 10^{\circ}\text{C}$ . This shows that for improving the cooling system the cooling itself as well as the transport of the cooling fluid have to be improved. In addition the temperature gradient caused by cooling liquid flow  $\Delta T_{flow} = 11^{\circ}\text{C}$  can be analysed in more detail. The biggest part of  $6^{\circ}\text{C}$  is caused by heating of the cooling liquid outside the vacuum chamber. Inside the vacuum chamber the cooling liquid is heated up by an additional  $2^{\circ}\text{C}$  before it reaches the cooling structure. Finally there is a  $2^{\circ}\text{C}$  difference between the cooling liquid and the copper cooling structure. This temperature gradient between cooling liquid and copper was counted to the  $\Delta T_{flow}$  because it is not influenced by the heating power of the silicon.

With the thermal conductance of the direct cooling for the pion tracker detector ( $\sigma_{Q,PT}^{indirect} = 75 \text{ mW/K}$ , see 3.3.1) the total heating power to the silicon is approximately  $750 \text{ mW}$ . This more or less fits to the expected heating by thermal radiation  $P_{PT}^{AR} = 200\text{--}470 \text{ mW}$ . The nonconformity of approximately 40% could be caused by inaccuracies of the emissivity of the detector surface used to estimate the heating

power of the ambient radiation. Or the inaccuracies of the thermal conductivity of FR4 used to simulate the thermal conductance of the PCB.

### 6.3 Influence of reflecting foil

The influence of the reflecting foil can be analysed by comparing the temperature gradient copper-silicon for the setup with and without reflecting foil. The difference  $\Delta T_{foil} = \Delta T_{copper-silicon,with\ foil} - \Delta T_{copper-silicon,without\ foil}$  can be seen in figure 6.5.

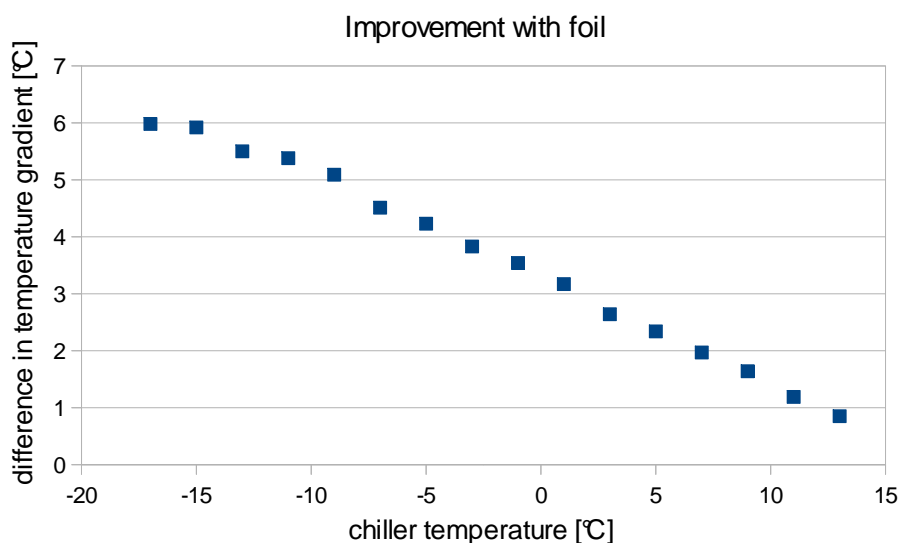


Figure 6.5: The reduction of the temperature difference between copper cooling structure and silicon due to a foil, which reflects thermal radiation.

The difference  $\Delta T_{foil}$  is approximately 6°C at  $-17^{\circ}\text{C}$  chiller temperature. So the temperature gradient  $\Delta T_{conduct}$  is reduced by 60%. The remaining temperature gradient is comparable to the temperature gradient between copper and silicon of the first prototype of an direct cooling system. The temperature of the silicon for the indirect cooling with foil (see figure 6.3) reached  $-1^{\circ}\text{C}$ . Additionally the huge temperature gradient in the cooling liquid flow can be reduced using the approaches discussed in section 5.2.



## 7 Summary and Outlook

In order to make a final conclusion, the most important results of the different considerations and the prototype measurements are summarised. The performance of a cooling system was evaluated by looking at two different temperature gradients. On the one hand, the temperature gradient  $\Delta T_{flow}$  between the chiller and the cooling structure, which is caused by the cooling liquid flow, and on the other hand, the temperature gradient  $\Delta T_{conduct}$  between the cooling structure and the silicon detector, which is caused by heat conduction.

### Summary of aspects concerning $\Delta T_{conduct}$

An estimation of  $\Delta T_{conduct}$  was done by analysing following three central characteristics:

**Heating power of the silicon:** The amount of heat that must be dissipated in the pion tracker setup was theoretically estimated to 380 – 780 mW (chapter 3.2). This is almost entirely given by ambient heat radiation (200 – 470 mW) and heat conduction through readout cables (180 – 310 mW). The tests with the indirect cooling prototype suggested that the heating power due to ambient heat radiation could be in fact up to 40% higher (chapter 6.2), which would lead to a heating power of up to 970 mW.

**Reducing heating power:** Additionally, possibilities to reduce the heating to the detector were analysed. With the different methods described in chapter 5.1.2 the heating could be significantly reduced. In an experimental test with a mylar foil (chapter 6.3) a reduction of heating by ambient heat radiation of 60% was observed. A combination of the different methods should further reduce the heating by ambient heat radiation and completely avoid heating through the readout cables. This could reduce the heat that must be dissipated to 260 mW.

**Thermal conductance:** The thermal conductance between the cooling structure and the silicon was calculated for two different approaches of a cooling system. The direct cooling maximises the thermal conductance by bypassing the detector PCB with a direct contact to the silicon, which leads to  $\sigma_Q^{direct} = 3.92 \frac{\text{W}}{\text{K}}$  (chapter 5.1.1). The indirect cooling just cools by heat conduction via the detector PCB to minimise problems caused by mechanical pressure on the silicon. The thermal conductance was estimated to  $\sigma_Q^{indirect} = 75 \frac{\text{mW}}{\text{K}}$  (chapter 3.3.1).

Thus, for a direct cooling the reduction of the heating power is unnecessary since the temperature gradient  $\Delta T_{conduct}$  is lower than  $1^\circ\text{C}$  even without it. To be able to have a reasonable indirect cooling, a reduction of the heating power is inevitable. By using all methods of reducing heating power, which were discussed in this thesis, the temperature gradient could be reduced to  $\Delta T_{conduct} = 3\text{--}4^\circ\text{C}$ .

### Summary of aspects concerning $\Delta T_{flow}$

The temperature gradients  $\Delta T_{flow}$  observed in the two prototype tests were  $5^\circ\text{C}$  (chapter 4.2) and  $11^\circ\text{C}$  (chapter 6.2). Both are higher than the temperature gradients caused by the two different cooling system designs. To reduce this temperature gradient is important for the direct as well as the indirect cooling. This can be done by improving the isolation of the cooling liquid pipes and by increasing the cooling liquid flow (chapter 5.2). The most promising approach is to increase the cooling liquid flow, since in both prototype setups that were evaluated here, the cooling liquid circuit was completed by using narrow pipes. This was done because narrow pipes can be bent more easily, making it possible to directly start measuring the behavior of the cooling structure without having to wait for customised pipes to be made. Using customised pipes could increase the cooling liquid flow by a factor of 3 or 4, reducing the temperature gradient by the same amount.

Taking all these aspects into account, the central result of this thesis is that a cooling system reaching the targeted temperature range can be realised with both cooling structure designs.

The next step will be to build an optimised cooling liquid circuit. This should make it possible to cool the silicon to the desired temperature range and to investigate how to run the cooling system over a longer timescale. Additionally the effect of the thermal stress caused by the different thermal expansion coefficients of silicon and FR4 has to be estimated for the indirect cooling. This can be done by measuring the leakage current of a pion tracker detector over the whole temperature range of the chiller. After that, a decision between the direct and indirect cooling structure has to be made. In the case that the indirect cooling performs well in combination with an optimised cooling liquid circuit and there are no negative effects caused by the thermal stress, the decisive factor for the decision will be the problems caused by mechanical pressure on the silicon. In addition, the indirect cooling structure has to be supplemented with a fridge that is topped with a reflecting foil (chapter 5.1.2), and also with a device to cool the readout cables.

---

## Bibliography

- [1] G. Agakichiev et al. (HADES Coll.), *The European Physical Journal A* 41, 243-277, 2009.
- [2] J. Wirth, *Development of a cooling system for a silicon particle detector*, Bachelor Thesis, Technische Universität München, 2012.
- [3] T. Schmitt, *Tracking studies with silicon detectors for the HADES Pion Tracker*, Bachelor Thesis, Technische Universität München, 2013.
- [4] E. Barberis et al., *Temperature effects on radiation damage to silicon detectors*, *Nuclear Instruments and Methods in Physics Research A* 326, 373-380, 1993.
- [5] J. H. Lienhard IV, J. H. Lienhard V, *A heat transfer textbook*, Phlogiston Press, Cambridge, 3rd edition, 2008.
- [6] R. Gross, A. Marx, *Festkörperphysik*, Oldenbourg Wissenschaftsverlag, München, 2012.
- [7] M. Friedl, *The CMS silicon strip tracker and its electronic readout*, Doctor Thesis, Vienna University of Technology, 2001.
- [8] Emissivity Coefficients of some common Materials, [www.engineeringtoolbox.com/emissivity-coefficients-d\\_447.html](http://www.engineeringtoolbox.com/emissivity-coefficients-d_447.html) (29.07.2013).
- [9] M. J. Winter, Physical properties, [www.webelements.com/physics.html](http://www.webelements.com/physics.html) (29.07.2013).
- [10] A. Hammer, H. Hammer, K. Hammer, *Physikalische Formeln und Tabellen*, J. Lindauer Verlag, München, 8. Auflage, 2002.
- [11] A. van Oosterom, J. Strackee, *The Solid Angle of a Plane Triangle*, *IEEE Transactions on Biomedical Engineering BME-30 Issue: 2*, 125-126, 1983.



# Appendix

## Material data

copper		
thermal conductivity $\lambda$ [9]		$400 \frac{\text{W}}{\text{m}\cdot\text{K}}$
specific heat capacity $c$ [10]		$0.385 \frac{\text{J}}{\text{g}\cdot\text{K}}$
mass density $\rho$ [10]		$8.93 \frac{\text{g}}{\text{cm}^3}$
emissivity $\varepsilon$	highly polished [8]	0.023–0.052
	slightly polished [5]	0.12–0.15
	black oxidised [5]	0.76

aluminium		
thermal conductivity $\lambda$ [9]		$235 \frac{\text{W}}{\text{m}\cdot\text{K}}$
specific heat capacity $c$ [10]		$0.896 \frac{\text{J}}{\text{g}\cdot\text{K}}$
mass density $\rho$ [10]		$2.70 \frac{\text{g}}{\text{cm}^3}$
emissivity $\varepsilon$	highly polished [8]	0.039–0.057
	commercial sheet [5, 8]	0.09
	heavily oxidised [5]	0.20–0.33

iron		
thermal conductivity $\lambda$ [9]		$80 \frac{\text{W}}{\text{m}\cdot\text{K}}$
specific heat capacity $c$ [10]		$0.452 \frac{\text{J}}{\text{g}\cdot\text{K}}$
mass density $\rho$ [10]		$7.86 \frac{\text{g}}{\text{cm}^3}$

silicon		
thermal conductivity $\lambda$ [9]		$150 \frac{\text{W}}{\text{m}\cdot\text{K}}$
specific heat capacity $c$ [5]		$0.705 \frac{\text{J}}{\text{g}\cdot\text{K}}$
mass density $\rho$ [9]		$2.33 \frac{\text{g}}{\text{cm}^3}$
emissivity $\varepsilon$	silicon carbide [8]	0.83–0.96

FR 4		
thermal conductivity $\lambda$ [5]		$0.29 \frac{\text{W}}{\text{m}\cdot\text{K}}$
specific heat capacity $c$ [5]		$\sim 1.6 \frac{\text{J}}{\text{g}\cdot\text{K}}$
mass density $\rho$		$1.8\text{--}1.9 \frac{\text{g}}{\text{cm}^3}$

kapton	
thermal conductivity $\lambda$	0.12–0.37 $\frac{\text{W}}{\text{m}\cdot\text{K}}$
specific heat capacity $c$	1.09 $\frac{\text{J}}{\text{g}\cdot\text{K}}$
mass density $\rho$	1.42 $\frac{\text{g}}{\text{cm}^3}$

delrin	
thermal conductivity $\lambda$	0.30–0.37 $\frac{\text{W}}{\text{m}\cdot\text{K}}$
specific heat capacity $c$	1.42 $\frac{\text{J}}{\text{g}\cdot\text{K}}$
mass density $\rho$	7.86 $\frac{\text{g}}{\text{cm}^3}$

Thermipad® TP 22600	
thermal conductivity $\lambda$	1.0 $\frac{\text{W}}{\text{m}\cdot\text{K}}$
mass density $\rho$	2.0 $\frac{\text{g}}{\text{cm}^3}$
breakdown strength $E_{d;ac}$	$\geq 6.0 \frac{\text{kV}}{\text{mm}}$

Keratherm®-Softtherm®, 86/600	
thermal conductivity $\lambda$	6.0 $\frac{\text{W}}{\text{m}\cdot\text{K}}$
mass density $\rho$	1.28 $\frac{\text{g}}{\text{cm}^3}$
breakdown strength $E_{d;ac}$	3.0 $\frac{\text{kV}}{\text{mm}}$

## Root macro for Oosterom-Strackee algorithm

The Oosterom-Strackee algorithm [11] calculates the solid angle  $\Omega$  of a triangle seen from a specific point of view. The vectors  $\vec{a}$ ,  $\vec{b}$ ,  $\vec{c}$  are the vectors connecting the point of view to the edges of the triangle.  $a, b, c$  are the magnitudes of the vectors  $\vec{a}$ ,  $\vec{b}$ ,  $\vec{c}$ .

$$\tan\left(\frac{1}{2}\Omega\right) = \frac{\vec{a} \cdot (\vec{b} \times \vec{c})}{abc + (\vec{a} \cdot \vec{b})c + (\vec{a} \cdot \vec{c})b + (\vec{b} \cdot \vec{c})a}$$

Following root macro was used to calculate the average open solid angle seen from the silicon surface for different fridge heights.

```
//SolidAngle.C
void SolidAngle() {
//__The lengh of the detector is 100x100mm, grid defines the grid size__
const Int_t lenght = 100;
const Int_t grid = 500;

Double_t height;
TVector3 edge1;
```

```

TVector3 edge2;
TVector3 edge3;
TVector3 edge4;

TVector3 location;
TVector3 v1;
TVector3 v2;
TVector3 v3;
TVector3 v4;

//__Here the number of fridge hights is chosen__
const Int_t size = 20;
TCanvas *c1[size];

Double_t omega;
Double_t percent;
Double_t a1;
Double_t a2;
Double_t b1;
Double_t b2;

//__Here the fridge hights that are calculated are chosen__
for (Int_t k=0; k <= size; k++){
    height = 25 + 1*k;

    edge1.SetXYZ(.5*length,.5*length,height);
    edge2.SetXYZ(.5*length,-.5*length,height);
    edge3.SetXYZ(-.5*length,-.5*length,height);
    edge4.SetXYZ(-.5*length,.5*length,height);

    Double_t average = 0;
    TH2F* hist = new TH2F(TString::Format("Values for height %f mm",
height),TString::Format("Open solid angle for height %f mm",height),
grid,0,grid,grid,0,grid);
    hist->SetStats(0);

    for (Int_t i=0; i < grid; ++i){
        for (Int_t j=0; j < grid; ++j){
            location.SetXYZ((i+0.5)*0.5*length/grid,
(j+0.5)*0.5*length/grid,0);
            v1 = edge1 - location;
            v2 = edge2 - location;
            v3 = edge3 - location;
            v4 = edge4 - location;

```

```

        a1 = TMath::Abs(v1.Dot(v3.Cross(v4)));
        b1 = v1.Mag()*v3.Mag()*v4.Mag() +
(v1*v3)*v4.Mag() + (v1*v4)*v3.Mag() + (v3*v4)*v1.Mag();
        a2 = TMath::Abs(v1.Dot(v2.Cross(v3)));
        b2 = v1.Mag()*v2.Mag()*v3.Mag() +
(v1*v2)*v3.Mag() + (v1*v3)*v2.Mag() + (v2*v3)*v1.Mag();
        omega = 2*TMath::ATan2(a1,b1) + 2*TMath::ATan2(a2,b2);

        percent = omega * 100 / (2*TMath::Pi());
        hist->Fill(i,j,percent);
        average = average + percent;
    }
}
c1[k] = new TCanvas(TString::Format("hist%d",k),
"SolidAngle Simulation",1000,1000);
c1[k]->cd();
hist->Draw("colz");
c1[k]->Update();

average = average / (grid*grid);
cout << height << "\t" << average << endl;
}
}

```

# Acknowledgments

I would like to thank all the people without who this thesis would not have been possible. First of all Prof. Laura Fabbietti who gave me the freedom to test and investigate new ideas and approaches besides the simple straight way of handling this project. And of course Joana Wirth, who explained me every instrument and program I had to use. Without her experience and the time she sacrificed, I would have spent a lot of time learning everything by myself. Additionally Rafal Lalik who always helped me with programming issues and was a very precise and active proofreader. I would also like to thank Sonja Winkler, Dr. Roman Gernhäuser and Dr. Jürgen Friese, who were always willing to help with difficult questions and Ralf Lang and Michael Klöckner from the workshop who built the new prototype. Not to forget all others from the E12 Universe Cluster , and especially those from our office room, you all are responsible for the good and positive atmosphere.

Thank you !